Small emission sources in aggregate disproportionately account for a large majority of total methane emissions from the US oil and gas sector

James P. Williams[1], Mark Omara[1,2], Anthony Himmelberger[2], Daniel Zavala-Araiza[1], Katlyn MacKay[1], Joshua Benmergui[1,2,3], Maryann Sargent[3], Steven C. Wofsy[3], Steven P. Hamburg[1,2], Ritesh Gautam[1,2]

[1]Environmental Defense Fund, New York, NY, USA 10010
[2]MethaneSAT, LLC, Austin, TX, USA 78701
[3]Harvard University, Cambridge, MA, USA 02138

Correspondence to: James P. Williams (jamwilliams@edf.org), Ritesh Gautam (rgautam@edf.org)

Abstract. Reducing methane emissions from the oil and gas (oil/gas) sector has been identified as a critically important global strategy for reducing near-term climate warming. Recent measurements, especially by satellite and aerial remote sensing, underscore the importance of targeting the small number of facilities emitting methane at high rates (i.e., "super-emitters") for measurement and mitigation. However, the contributions from individual oil/gas facilities emitting at low emission rates that are often undetected are poorly understood, especially in the context of total national- and regional-level estimates. In this work, we compile empirical measurements gathered using methods with low limits of detection to develop facility-level estimates of total methane emissions from the continental United States (CONUS) midstream and upstream oil/gas sector for 2021. We find that 70% (95% confidence intervals: 61-81%) of the total 14.6 (12.7-16.8) Tg/yr oil/gas methane emissions in the CONUS for the year 2021 originate from facilities emitting <100 kg/hr, and 30% (26-34%) and ~80% (68-90%) from facilities emitting <10 kg/hr and <200 kg/hr, respectively. While there is variability among the emission distribution curves for different oil/gas production basins, facilities with low emissions are consistently found to account for the majority of total basin emissions (i.e., range of 60% - 86% of total basin emissions from facilities emitting <100 kg/hr). We estimate that production well sites were responsible for 70% of regional oil/gas methane emissions, from which we find the well sites that accounted for only 10% of national oil and gas production in 2021, disproportionately accounted for 67-90% of the total well site emissions. Our results are also in broad agreement with data obtained from several independent aerial remote sensing campaigns (e.g., MethaneAIR, Bridger Gas Mapping LiDAR, AVIRIS-NG, and Global Airborne Observatory) across 5-8 major oil/gas basins. Our findings highlight the importance of accounting for the significant contribution of small emission sources to total oil/gas methane emissions. While reducing emissions from high-emitting facilities is important, it is not sufficient for the overall mitigation of methane emissions from the oil and gas sector which according to this study is dominated by small emission sources across the US. Tracking changes in emissions over time and designing effective mitigation policies should consider the large contribution of small methane sources to total emissions.

38

1 Introduction

Methane is a short-lived but powerful greenhouse gas with a global warming potential more than 80 times stronger than carbon dioxide (CO_2) over 20 years (AR6 Synthesis Report: Climate Change 2023, 2024). Therefore, the reduction of methane emissions has become a key goal to achieve rapid climate mitigation in the short term (Ocko et al., 2021). In North America, one of the largest sources of methane emissions originates from the oil and gas (oil/gas) sector, with most emissions originating from the production (i.e., upstream) and transportation/storage (i.e., midstream) sectors (Alvarez et al., 2018). Multiple studies, especially over the past decade, have focused on the quantification of methane sources from the oil/gas sector, with particular emphasis on the continental United States (CONUS) (Alvarez et al., 2018; de Gouw et al., 2020; Omara et al., 2018; Lu et al., 2022; Zhang et al., 2020; Shen et al., 2022; Cusworth et al., 2022; Nesser et al., 2023; Brandt et al., 2016; Duren et al., 2019; Maasakkers et al., 2021; Lu et al., 2023; Worden et al., 2022). Several studies have recognized the importance of a small percentage of high-emitting sites (i.e. "super-emitters") and reported them as accounting for a large fraction of total methane emissions (Brandt et al., 2016; Cusworth et al., 2022; Duren et al., 2019; Sherwin et al., 2024). The emission rate thresholds that characterize these super-emitting facilities are critical information for methane measurement platforms, especially remote sensing technologies focused on detecting high-emitting point sources. Aerial and satellite remote sensing technologies have enabled more frequent monitoring of emissions from oil and gas sites and rapid mapping of large areas, although they face limitations in detection sensitivity. Despite the improved ability to locate and quantify emissions from high-emitting sites, there has been considerable lack of understanding about the characteristics of low methane emitting facilities, especially those emitting at rates below the limits of detection (LOD) of most point-source detection remote sensing platforms, and their contributions to total oil/gas methane emissions.

While some studies offer important yet limited insights into the contributions of different lower-emitting infrastructure from the CONUS oil/gas sector, there is a lack of understanding about their overall contribution to the total sectoral regional and national scale emissions. A recent study by Xia et al. (2024) combined aerial remote sensing data from Bridger Gas Mapping LiDAR (Bridger GML) in four oil/gas basins supplemented with component-level modeling for facilities emitting below the Bridger GML LOD and found significantly more emission sources in the 1 – 10 kg/hr range when compared to the emission distribution used by the EPA (Xia et al., 2024). In a study focused on production well sites in the CONUS, the main source of methane emissions from the oil/gas sector (Alvarez et al., 2018; Omara et al., 2018; Rutherford et al., 2021), Omara et al. (2018) found that 90% of total methane emissions from producing well sites came from those emitting at rates <100 kg/hr. A follow-up study by Omara et al. (2022) highlights that the total methane emissions from low-producing well sites producing less than 15 boe/day (i.e., 1 Mcf = 1,000 cubic feet of natural gas = 19.2 kg of methane at 15.6 °C and 1 atmosphere; 1 boe = 1 barrel of oil equivalent = 6 Mcf; assumed methane content in natural gas of 80%), which comprise 80% of

73 all producing well sites in the CONUS, were responsible for nearly half of all methane emissions from the oil/gas

74 production sector. Kunkel et al. (2023) observed that the use of the Bridger GML remote sensing platform with an

75 LOD of 3 kg/hr, combined with prior Carbon Mapper detections in a section of the Permian basin showed a

76 significant contribution from sources below the listed LOD of Carbon Mapper of 10 kg/hr. Cusworth et al. (2022)

77 found that 35% of total methane emissions (including non-oil/gas sources) from several major oil/gas producing

78 basins (other than the Appalachian basin) in the CONUS come from facilities emitting >10 kg/hr, indicating that

79 65% of emissions come from facilities emitting <10 kg/hr. Although these studies using independent measurement

80 platforms provide new emerging insights about the importance of low methane emitting oil/gas facilities, there

81 generally remains a lack of quantitative assessment of the relative fractions of emissions originating from different

82 emission rate thresholds aggregated over individual oil/gas basins as well as at a national scale.

83 There are a variety of different methane quantification methods that differ in terms of their spatial resolution of

84 sources, logistical constraints, costs of implementation, and their LODs. Measurement method sensitivities and

85 LODs have important policy implications. For example, the Environmental Protection Agency (EPA) recently

86 finalized regulations that define a "super-emitter event" as an emission rate threshold of 100 kg/hr or greater

87 (Standards of Performance for New, Reconstructed, and Modified Sources and Emissions Guidelines for Existing

88 Sources: Oil and Natural Gas Sector Climate Review, 2024), albeit without clear information on what percentage of

89 total regional emissions are captured within this definition. Satellite and aerial remote sensing methods have point

90 source LODs that range anywhere from 1-3 kg/hr for Bridger's airborne GML (Johnson et al., 2021; Kunkel et al.,

91 2023; Thorpe et al., 2024; Xia et al., 2024) to ~200 kg/hr for GHGSat (Sherwin et al., 2023). In contrast, ground-

92 based measurement methods such as OTM-33a and tracer release have LODs <1 kg/hr (Fox et al., 2019). A study by

93 Ravikumar et al. (2018) using the Fugitive Emissions Abatement Simulation Toolkit (FEAST) suggests that a

94 method with a LOD of 0.1-1 kg/hr would sufficiently capture all emissions from the oil/gas sector, whereas the

95 ability to quantify emissions below this threshold would not lead to any significant increases in mitigation.

96 Ultimately, there is a need for clarification in the total percentage contribution of emissions originating from a given

97 emission rate threshold, which requires characterizing entire emissions distributions, not only the high emitters.

98 In this work, we create and analyze measurement-based methane emission rate distributions of US upstream and

99 midstream oil/gas facilities to determine the percentage contributions of different emission rate thresholds to total

100 methane emissions. First, we use empirical measurements gathered from ground-based sampling platforms to

101 develop a bottom-up facility-based model to estimate methane emissions for upstream and midstream facilities in

102 the continental US (CONUS) for 2021. Next, we aggregate our facility-level, population-based data to determine the

103 national- and basin-level contributions of methane emissions originating from facilities emitting at different

104 emission rate thresholds, in addition to comparisons to aerial-remote sensing platforms. Finally, we break down the

105 emission distribution curves by facility category to analyze how the percentage contributions of total emissions vary

106 across facility types.

107

2 Materials and methods

2.1 Empirical measurements

We compile 1,901 facility-level methane emission rate measurements from 16 studies (Brantley et al., 2014; Caulton et al., 2019; Deighton et al., 2020; Goetz et al., 2015; Lan et al., 2015; Mitchell et al., 2015; Omara et al., 2016, 2018; Rella et al., 2015; Riddick et al., 2019; Robertson et al., 2017, 2020; Subramanian et al., 2015; Yacovitch et al., 2015; Zhou et al., 2021; Zimmerle et al., 2020) that use ground-based site/facility level and source/component level measurement methods with low LOD's of ~0.1 kg/hr. Most (i.e., 85%) of empirical measurements we use in this work were gathered using ground-based mobile laboratories that quantified methane emissions at the site/facility level using either tracer-based releases, the EPA Other Test Method (OTM-33a), or Gaussian plume transport modeling (Fox et al., 2019) (Table S2). The remaining 15% of empirical measurements we use (Deighton et al., 2020; Riddick et al., 2019; Zimmerle et al., 2020) are ground-based methods that aggregated source/component-level HiFlow sampling or static/dynamic chamber measurements, which could mean that other on-site emission sources were not quantified during measurement and overall emission rate estimates are conservative. Only one study was excluded from our analysis (ERG, 2011) due to a combination of age and a focus on component-level measurements.

The compiled empirical measurements target a variety of production well sites and/or midstream facilities across at least nine oil/gas-producing basins in the CONUS (Table S3). For all facility categories (i.e., production well sites, gathering and boosting compressor stations, transmission and storage compressor stations, and processing plants), we prioritize datasets of randomly sampled sites that include measurements below the method's LOD or reported as zero emissions, except for measurements from two studies (Brantley et al., 2014; Lan et al., 2015) which we discuss later in Section 2.3. Additionally, for production well site measurements, we focus only on data that provide facility-level gas production data for the date/month of measurement. Our compiled dataset of measurements includes both routine intentional (e.g., venting from pneumatic devices) and non-intentional (e.g., malfunctioning equipment and/or leaks from valves, connectors, flanges, etc) emissions, and while we remove any measurements attributed to high emitting intermittent events such as flowbacks and liquids unloadings if that information is present, we cannot fully discount that emissions from these high-emitting intermittent sources are included in our compiled dataset. Furthermore, we remove any empirical measurement data associated with flaring emissions, which are treated separately as discussed below, if that information is provided in the empirical data.

We categorize the empirical measurements by facility category as production well sites, gathering and boosting compressor stations (G&B compressors), transmission and storage compressor stations (T&S compressors), or processing plants. We group the empirical measurements from production well sites into six production bins based on gross average daily gas production as reported in individual studies. We use gross daily average gas production data instead of oil and gas production data for two reasons: 1) the limited availability of facility-level oil production data provided from empirical measurement studies; and 2) the established relationship between gas production and

emission rates observed in previous work (Omara et al., 2018, 2022, 2024). The gas production ranges of the production bins (Fig. 1) are chosen to evenly distribute empirical measurements above the method LOD to all six production bins. This categorization creates nine distinct facility categories: G&B compressors, T&S compressors, processing plants, and six groups of production well sites. We further classify the nine distinct facility categories into five primary facility categories: low-production well sites which produce combined oil and gas <15 boe/day (i.e., 0.13 kt of methane production per year), non-low-producing well sites which produce ≥15 boe/day, processing plants, G&B compressors, and T&S compressors. In addition to these facility categorizations, we also include Visible Infrared Imaging Radiometer Suite (VIIRS) flare detections and flared gas volume estimates in our analysis, which are treated as an independent methane source since flares can be located on multiple facility categories across the upstream and midstream oil/gas sectors.
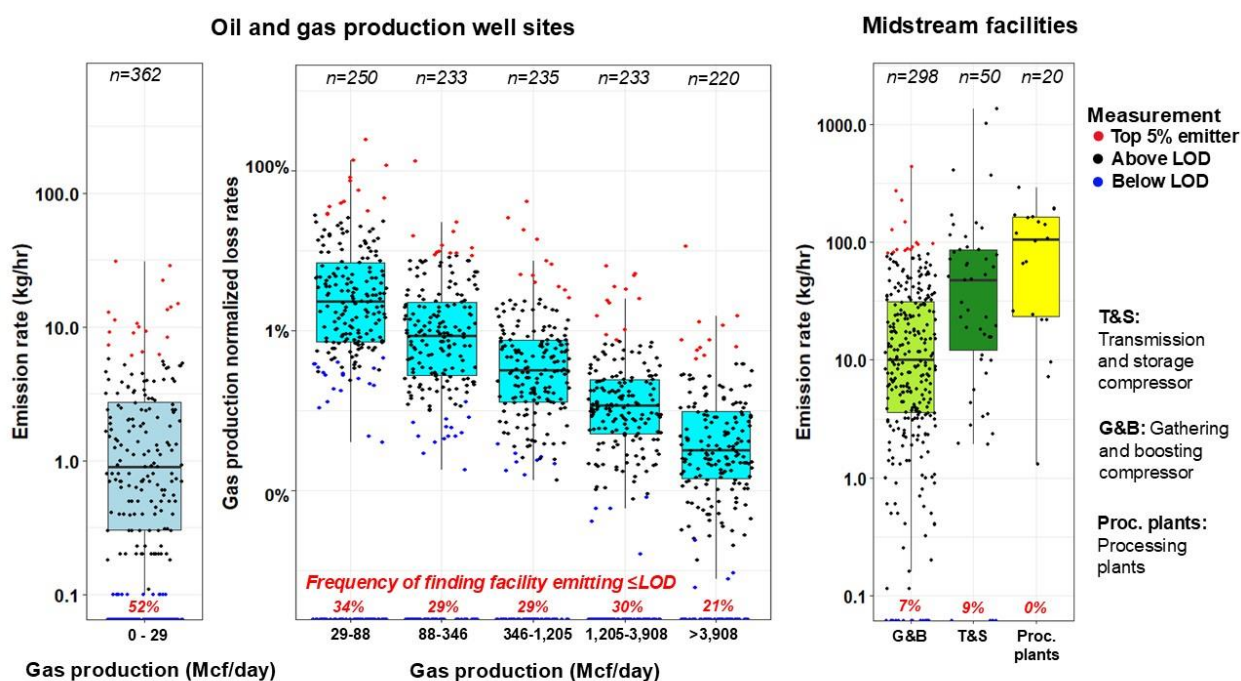
Figure 1: Facility-level empirical measurement data distributed by different distinct facility categories for production well sites (left) and midstream facilities (right). Individual measurements are shown for each box plot and colored according to their emission rate status for that facility category, where blue points are considered non-detectable emissions below an emission rate threshold of ≤0.1 kg/hr/facility which is the method LOD we use, black points are measurements above our method LOD but below the top 5% emitter category, and red points are the top 5% of empirical emission rates or loss rates for that facility category. The number of empirical measurements available for each facility category is denoted at the top of each boxplot. The estimated mean frequency of finding a facility emitting below the method LOD is shown in inset red text at the bottom of each boxplot We show absolute emission rates (kg/hr) rather than normalized loss rates (%) for the lowest cohort of production well sites due to the reasoning presented in Section 2.3. Unit conversions: 1 Mcf = 1,000 cubic feet of natural gas = 19.2 kg of methane at 15.6 °C and 1 atmosphere; 1 boe = 1 barrel of oil equivalent = 6 Mcf; assumed methane content in natural gas of 80%.

2.2 Activity data

168   We use activity data (i.e., number of facilities and spatial locations) for actively producing wells in 2021

169 provided by Enverus for the CONUS. We calculate both the annual averaged daily gross gas production, and oil and

170 gas production for each producing well using the number of producing days and total annual oil and gas production

171 data provided by Enverus. We convert production wells to production well sites by spatially aggregating individual

172 wells within 25-meter (vertical wells) or 50-meter (horizontal wells) distances from each other and separately

173 merging their combined oil and gas production and gas production, and converting these production values to a mass

174 equivalent production rate in kg/hr of methane (i.e., 1 Mcf = 1,000 cubic feet of natural gas = 19.2 kg of methane at

175 15.6 °C and 1 atmosphere; 1 boe = 1 barrel of oil equivalent = 6 Mcf; assumed methane content in natural gas of

176 80%), similar to previous approaches (Omara et al., 2018).

177   We acquire activity data for operational transmission and storage (T&S) and gathering and boosting (G&B)

178 compressor stations and processing plants from Enverus for 2021 for the CONUS, which was further supplemented

179 by additional data from the Oil and Gas Infrastructure Mapping (OGIM) database published in Omara et al. (2023).

180 We filter data for these midstream facilities to include only active facilities in the year 2021. For VIIRS flare

181 detections, we use the 2021 natural gas flared volume estimates based on natural gas flaring detections provided by

182 the VIIRS instruments installed aboard satellite platforms which have a 750x750 meter source resolution (NOAA-20

183 and Suomi National Polar-orbiting Partnership) (Elvidge et al., 2015). In terms of potential double-counting between

184 the VIIRS flare detections and the empirical measurements we use in this work, the majority of VIIRS detections are

185 in the Permian, Bakken, and Eagle Ford oil/gas basins (i.e., 86% of total VIIRS detections) which corresponds to a

186 small number of our empirical measurement data (Table S3) (Plant et al., 2022). However, the limited availability of

187 spatial coordinates for our empirical measurements restricts our ability to perform a direct comparison to exclude

188 overlapping/proximal VIIRS detections and our facility-level empirical measurements. Therefore, we do

189 acknowledge that there is a possibility of double counting between our empirical measurement data and the VIIRS

190 flare detections, but we expect the degree of overlap to be low.

191 **2.3 Facility-level methane emission inventory**

192   We calculate annual methane emissions from all facility categories (i.e., six production bins of production well

193 sites, T&S compressor stations, G&B compressor stations, processing plants, and VIIRS flare detections) using a

194 multi-step probabilistic modeling approach adapted from multiple studies (Omara et al., 2018, 2022; Plant et al.,

195 2022) (Fig. 2). Briefly, for each individual facility and VIIRS flare detection in the CONUS for 2021, we estimate an

196 annually averaged methane emission rate using empirical measurement data, and consequently the cumulative

197 distribution of methane emission rates from the aggregation of these individual emission rates. Each emission rate

198 estimate is indexed according to the corresponding replicate (n=500), and we use these repetitions to determine

199 uncertainty for the cumulative methane emission distribution curves. The detailed steps of this process for all facility

200 categories and VIIRS flare detections are described below.

201   For the highest five gas production bins of producing well sites ranging from 29 to >3,908 Mcf/day (or 0.2 to

202 >27 kt of methane production per year, Figure 1), we use gross gas production normalized loss rates to model the

203 distributions used to calculate methane emission rates from Eq. (1), where the: *Loss rate* is the fraction of emitted

204 gas relative to gas production, the *emission rate* is rate of methane emitted from a facility in kilograms per hour,

205 σ_{CH4} is the methane content of the emitted gas which we assume to be 80%, and the *gas production* is the mass

206 equivalent of natural gas produced in kilograms per hour at 1 atmosphere and 15.6 °C (1 Mcf = 1,000 cubic feet of

207 natural gas = 19.2 kg of methane at 15.6 °C and 1 atmosphere; 1 boe = 1 barrel of oil equivalent = 6 Mcf). For the

208 lowest well site gas production bin of 0 to 29 Mcf/day (i.e, 0 to 0.2 kt of methane production per year) and

209 midstream facilities, we use the empirical absolute methane emission rate data as is. This approach is partly based

210 on the methods used by Omara et al. (2022) for the low production well site category, which exploits a weak

211 relationship between gross gas production data (which is most accessible in empirical measurement studies) and

212 absolute emission rates to better extrapolate emissions to the entire population of production well sites in the

213 CONUS.

214 $$Loss\ rate = \frac{Emission\ rate\ \left[\frac{kg}{hr}\right]}{\sigma_{CH_4} \times Gas\ production\ \left[\frac{kg}{hr}\right]} \quad (1)$$

215   For our estimation of facility-level emission rates, we break down the modeling process into two separate steps:

216 the first determines whether a randomly selected facility is emitting methane above our method LOD of ≤0.1

217 kg/hr/facility, and the second determines the associated methane emission rate for that individual facility. To test the

218 sensitivity of our method to the selection of the method LOD, we also perform an additional sensitivity analysis for

219 other method LODs (Fig. S8). The processes outlined below are all specific to each of our nine facility categories.

220 Brantley et al. (2014) and Lan et al. (2015) are excluded from this first step since they do not include measurements

221 below the method LOD but include valuable data on well site emission rates with associated well site production

222 data. To determine whether a facility is emitting methane above the method LOD threshold in our estimates, we first

223 use bootstrapping with replacement (n=1,000) of our empirical measurement data to simulate the frequency of

224 finding an individual facility emitting methane above the method LOD (i.e., ≤0.1 kg/hr/facility), which we call an

225 "emitting facility" or "emitter" herein (Fig. 2). The results of the bootstrapping procedure represent a normal

226 probability distribution from which we estimate the frequency of finding an emitting facility (i.e., above the method

227 LOD) with associated uncertainty bounds. Next, we remove the empirical measurements below the LOD and use

228 bootstrapping with replacement (n=1,000) on the above LOD empirical measurements to determine the probability

229 of an emitting facility being in the top 5% (i.e., 95th percentile or above of empirical measurement data) or bottom

230 95% (i.e., 95th percentile or below the empirical measurement data) of emitters, except for processing plants and

231 T&S compressors which had too few measurements (n=20 and n=50 respectively) to distinguish between the top 5%

232 and bottom 95% of emission or loss rates. Similar to the process of determining the frequency of finding an emitting

233 facility, we use the results of the bootstrapping to develop a normal probability distribution that classifies an

234 emitting facility as either a top 5% or bottom 95% emitter. This pseudo-random selection of a top 5% emitter within

235 each facility category accounts for the functional definition of abnormally large emissions (i.e., super-emitters) that

236 can be observed in all facility categories (including well sites in different production bins) (Zavala-Araiza et al.

237 2015, Brandt et al. 2016). We fit the results of the bootstrapping to two normal distributions: one for the top 5% of

238   emitters and one for the bottom 95% of emitters. We use the associated parameters of each normal distribution to

239   randomly determine whether a facility is emitting in the top 5% or bottom 95% of emitters. These steps are repeated

240   for each facility for each facility category in the CONUS.

241   At the end of the first step of this facility-level modeling process, all facilities in the CONUS are classified as

242   either a: bottom 95% emitter, top 5% emitter, or below the method LOD. Loss rates are used to calculate emission

243   rates for the top five highest production bins of well sites, whereas we directly estimate methane emission rates for

244   the well sites in the lower production cohort (Fig. 1), and for midstream facilities excluding VIIRS flare detections.

245   For facilities classified as the top 5% and bottom 95% of emitters, we estimate their methane emissions by first

246   fitting a lognormal distribution to the empirical measurement data, including measurements from Brantley et al.

247   (2014) and Lan et al. (2015), of either the gas production normalized loss rates or methane emission rates (Eq. 1),

248   depending on the facility category. Next, we use the parameters of the modeled distributions to randomly assign

249   either an emission or loss rate to a randomly selected facility (n=500), depending on its emitter status and facility

250   category. We test each estimated methane emission distribution to the associated empirical measurements and find a

251   good fit for all facility categories (Table S6). To account for facilities emitting below the method LOD, we

252   randomly assign an emission rate from re-sampling our dataset of empirical measurements below the method LOD

253   for that facility category. Finally, once all facilities are assigned an emission rate, we compile the ensemble of

254   emission distributions to develop facility-level emission distribution curves and total regional oil/gas methane

255   emissions for the CONUS in 2021.

256   For all VIIRS flares detections, we use the total reported volumes of gas flared for 2021 from flares detected

257   using the VIIRS instrument (Elvidge et al. 2015) multiplied by the observed flare destruction efficiencies and

258   percentage of unlit flares from Plant et al. (2022) to calculate annual methane emission rates from this source. As

259   previously stated, our empirical measurements are largely located outside of oil/gas basins where the majority of

260   VIIRS flare detections are located (i.e. Permian, Eagle Ford, and Bakken), but we cannot discount the possibility

261   that there are instances of double-counting flares measured via our ground-based empirical data and those detected

262   by VIIRS. For each VIIRS flare detection, we randomly determine whether it is an unlit or lit flare based on the

263   basin-specific percentages of unlit flares reported by Plant et al. (2022). If a flare is determined to be lit, we use the

264   corresponding basin-specific observed destruction removal efficiencies as reported by Plant et al. (2022) multiplied

265   by the corresponding annual total volume of gas flared and convert to an emission rate. The basin-specific observed

266   destruction removal efficiencies are estimated through a fitted normal distribution using the mean and standard

267   deviations modeled from the 95% confidence intervals presented in Plant et al. (2022). If a flare is determined to be

268   unlit, we use a destruction removal efficiency of 0%. For VIIRS flare detections located outside of the Bakken,

269   Eagle Ford, and Permian basins, we used the total CONUS averaged destruction removal efficiencies of 95.2%

270   (95% confidence interval: 94.3 – 95.9%) and percentage of unlit flares of 4.1% as reported by Plant et al. (2022).

271
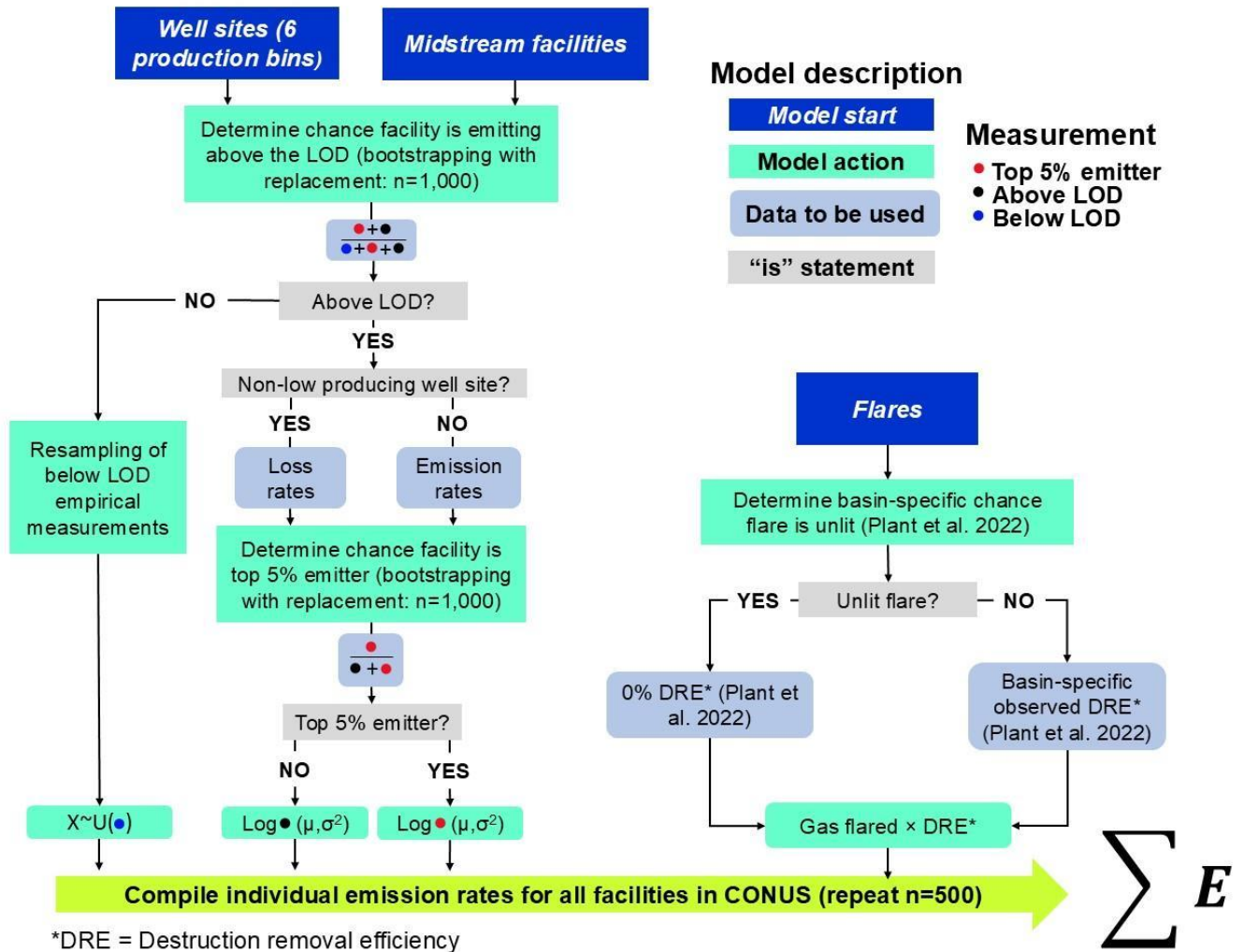
Figure 2: Flowchart describing the facility-level estimates, with steps colored according to the specific process and data being used. We note that methane emission rates for flares are calculated using a separate approach from that of production well sites and midstream facilities. Processing plants and T&S compressors are excluded from the determination of whether a facility is a top 5% emitter due to a lack of available empirical measurement data.

2.4 Extrapolation to smaller spatial boundaries

We perform several comparisons of our estimated emission distribution curves and total aggregated emissions to estimates from aerial and satellite remote-sensing studies. To perform these comparisons, we restrict our estimates and the results from other aerial/satellite studies to spatial domains of interest (e.g., an oil/gas basin boundary or the overflown domain from an aerial sampling campaign), and to specifically compare estimates of oil/gas methane emissions from the facility categories we are investigating in this work. For comparisons to satellite remote-sensing studies, we prioritize national-level satellite inversions that estimate methane emissions from the CONUS that include spatially explicit maps of methane emission inversions specifically for oil/gas sources. We join the spatially explicit satellite inversions of methane emissions to the top twelve producing oil/gas basin boundaries

288 in the CONUS, in addition to their national-level inversions which we also use for national comparisons. Since our

289 facility-level model includes geo-located activity data (i.e., facility coordinates), we can estimate facility-level

290 methane emissions distributions and estimate total methane emissions for any spatial boundary in the CONUS by

291 spatially joining facilities within a target boundary. Spatial variability in our facility-level estimates is driven by two

292 main factors: counts of facilities and facility types, and averaged annual production characteristics. Due to

293 constraints on data availability, we do not constrain our available empirical measurement data to the specific regions

294 where they were gathered (Table S3). We tested the sensitivity of excluding empirical measurements gathered from

295 specific oil/gas on the national emission distribution curves and total national methane emissions and found no

296 significant variation (Fig. S9). Due to a lack of data availability, we do not have sufficient spatial information from

297 empirical measurements of G&B compressors, T&S compressors, and processing plants to test for basin-level

298 differences in empirical measurement data.

299   For comparisons to aerial remote sensing studies/results, we prioritize studies that include both measured

300 point sources (i.e., oil/gas methane sources that are above the LOD of the aerial remote sensing measurement

301 platform), estimates of total regional oil/gas emissions, and descriptions/outlines of the surveyed spatial domains

302 which are required for these comparisons. Based on these criteria, we compare our estimated emissions to those

303 from peer-reviewed studies (Cusworth et al., 2022; Kunkel et al., 2023; Xia et al., 2024) and the results of research

304 flights from MethaneAIR in the Permian and Uinta oil/gas basins (Omara et al., 2024; Chan Miller et al., 2023;

305 Chulakadabba et al., 2023; MethaneAIR, 2024), with discussion in later sections on a recent study by Sherwin et al.

306 (2024). In all cases, we estimate facility-level methane emissions within the spatial domains outlined by the aerial

307 remote sensing studies to estimate region-specific methane emission distribution curves, use the relevant method

308 limits of detection to characterize emission rate thresholds valid for comparison, and subtract any emission unrelated

309 to the facility types we characterize (Chen et al., 2024). In the case of Cusworth et al. 2022, we infer the spatial

310 domains by georeferencing figures from their studies using the georeferencer tool QGIS (v.3.34.2-Prizen). We

311 compare our spatially joined facility-level emission distributions to the percentage of emissions contributed from

312 facilities emitting below discrete methane emission rate thresholds for all four aerial remote sensing studies, and to

313 the continuous cumulative methane emissions distribution curves from Bridger GML surveys (Kunkel et al., 2023;

314 Xia et al., 2024).

315   Each aerial remote sensing campaign utilizes independent methods to estimate their percentage

316 contributions from small methane sources, which in some cases requires additional analysis of the aerial remote

317 sensing results. For our analysis of continuous methane emissions distribution curves from the Bridger GML

318 campaigns (Kunkel et al., 2023; Xia et al., 2024), we restrict our analysis to estimated emission rates >3 kg/hr,

319 which is the approximate LOD of the Bridger GML remote sensing platform. For MethaneAIR, we use the

320 percentage of area emissions (i.e., diffuse area methane sources) relative to the total methane emissions for the

321 spatial boundary, which roughly corresponds to all emissions <200 kg/hr (i.e. effectively those emissions below the

322 point source detection limit of MethaneAIR that flew in multiple campaigns in the US at 40,000ft above ground

323 level (Chulakadabba et al., 2023)). MethaneAIR characterizes the total regional emissions including the spatial area

324 emissions at high resolution using a geostatistical inverse modeling framework (Miller et al., 2013) while ingesting
325 high-emitting point source information in the inversion (Chulakadabba et al., 2023; Omara et al., 2024). For
326 Cusworth et al. (2022), we analyze all campaigns by subtracting both aerially detected pipeline emissions and all
327 non-oil/gas emissions (e.g., wastewater, landfills, agriculture), since our study is focused solely on upstream and
328 midstream oil/gas sources. In addition, we subtract emissions from pipelines and non-oil/gas sources emitting below
329 aerial detection limits (i.e., TROPOMI inversions subtracted by aerially detected emissions) by estimating the
330 relative fractions of pipeline and non-oil/gas sources from the aerial detections, with the assumption that these
331 fractions are representative (Table S4). However, this process can introduce additional uncertainties in our
332 comparisons, especially for campaigns where 50% or more of aerially detected emissions were from pipelines or
333 non-oil/gas sources.

334   We account for the intermittency of detected methane sources with <3 overpasses in Cusworth et al.
335 (2022) by resampling with replacement (n=1,000) the source persistence of methane sources with ≥3 overpasses for
336 the same campaign, which is consistent with their methodology. We calculate the percentage contributions of low
337 emitting sources in Cusworth et al. (2022) using Eq. (2): where $\%E_{[<x]}$ is the percentage of total oil/gas methane
338 emissions below an emission rate threshold x (kg/hr), T is the total area emissions measured via TROPOMI
339 inversions (kg/hr), and $P_{[>x]}$ is the sum of point source emissions above the emission rate threshold x (kg/hr).

340 $$\%E_{[<x]} = 1 - \frac{P_{[>x]}}{T} \qquad\qquad (2)$$

341
342 **2.5 Uncertainty calculations**
343

344   Our emission distributions based on facility-level estimates incorporate uncertainty through several steps, such
345 as the: probabilistic distributions of a select facility being a top 5%, bottom 95% emitter, or facility emitting below
346 the LOD; emission rate and loss rate distributions produced from facility-level empirical measurements; and flaring
347 combustion efficiencies. In addition, we incorporate uncertainties from the empirical measurements into our facility-
348 level model by simulating new empirical emission rates based on the associated method uncertainties. At the
349 beginning of each of the 500 model iterations, we use the reported empirical methane emission rate data and
350 estimate a new emission rate using a normal distribution with the mean as the initial reported emission rate and the
351 standard deviation as a percentage of the mean value. These measurement uncertainties (i.e., 1-sigma) are chosen
352 based on the measurement methodology using the lower percentage uncertainty ranges provided by Fox et al. (2019)
353 for facilities measured via the OTM-33a (±25%), Gaussian plume dispersion (±50%), and tracer release (±20%)
354 methods. For HiFlow sampler measurements, we use an uncertainty range of ±16% (Riddick et al., 2022), and for
355 chamber-based measurements, we use ±14% (Williams et al., 2023). Therefore, each model iteration incorporates a
356 unique suite of empirical measurement data based on the initially reported emissions and their associated
357 uncertainties, which in turn impacts the probabilistic modeling of the chance of a facility emitting below the method
358 LOD, the empirical data is used to determine the parameters of the lognormal distributions of loss rates and emission

359 rates, and the ranges of the production bins. To calculate the cumulative uncertainty of our facility-level model

360 estimates, we estimate 500 methane emission distributions and aggregate the 2.5th and 97.5th percentiles of our seven

361 primary facility categories (i.e., low and non-low producing well sites, G&B compressors, T&S compressors, and

362 processing plants), which include lit and unlit VIIRS flare detection emissions, to determine our 95% confidence

363 intervals. This process is repeated for all simulations at the national-, basin-, and aerial remote sensing boundary

364 levels. For uncertainty calculations in satellite- and aerial-remote sensing studies we use for comparisons, we present

365 the reported 95% confidence intervals, if available.

366

367 **3 Results**

368

369 **3.1 Distribution of emission rates at the national scale**

370

371 Based on the results from our facility-level model estimates, we estimate that 70% (95% confidence

372 interval: 61-81%) of total methane emissions from the upstream/midstream sector in the CONUS for 2021 originate

373 from facilities emitting methane at rates <100 kg/hr (Fig. 3). For other emission rate thresholds, we find that 30%

374 (26-34%) of total emissions come from facilities emitting <10 kg/hr, which corresponds to the lower thresholds of

375 aircraft-based aerial remote sensing studies (Cusworth et al., 2022; Johnson et al., 2021; Kunkel et al., 2023; Thorpe

376 et al., 2024; Xia et al., 2024), and 79% (68-90%) of total emissions come from facilities emitting <200 kg/hr. We

377 find that the emission rate threshold corresponding to 50% of cumulative methane emissions from

378 upstream/midstream facilities in the CONUS for year 2021 is 25 kg/hr (19-33 kg/hr). These results suggest that a

379 large majority of oil/gas emissions in the CONUS are not detectable by existing satellite remote-sensing point

380   source imagers (Sherwin et al., 2023).

381
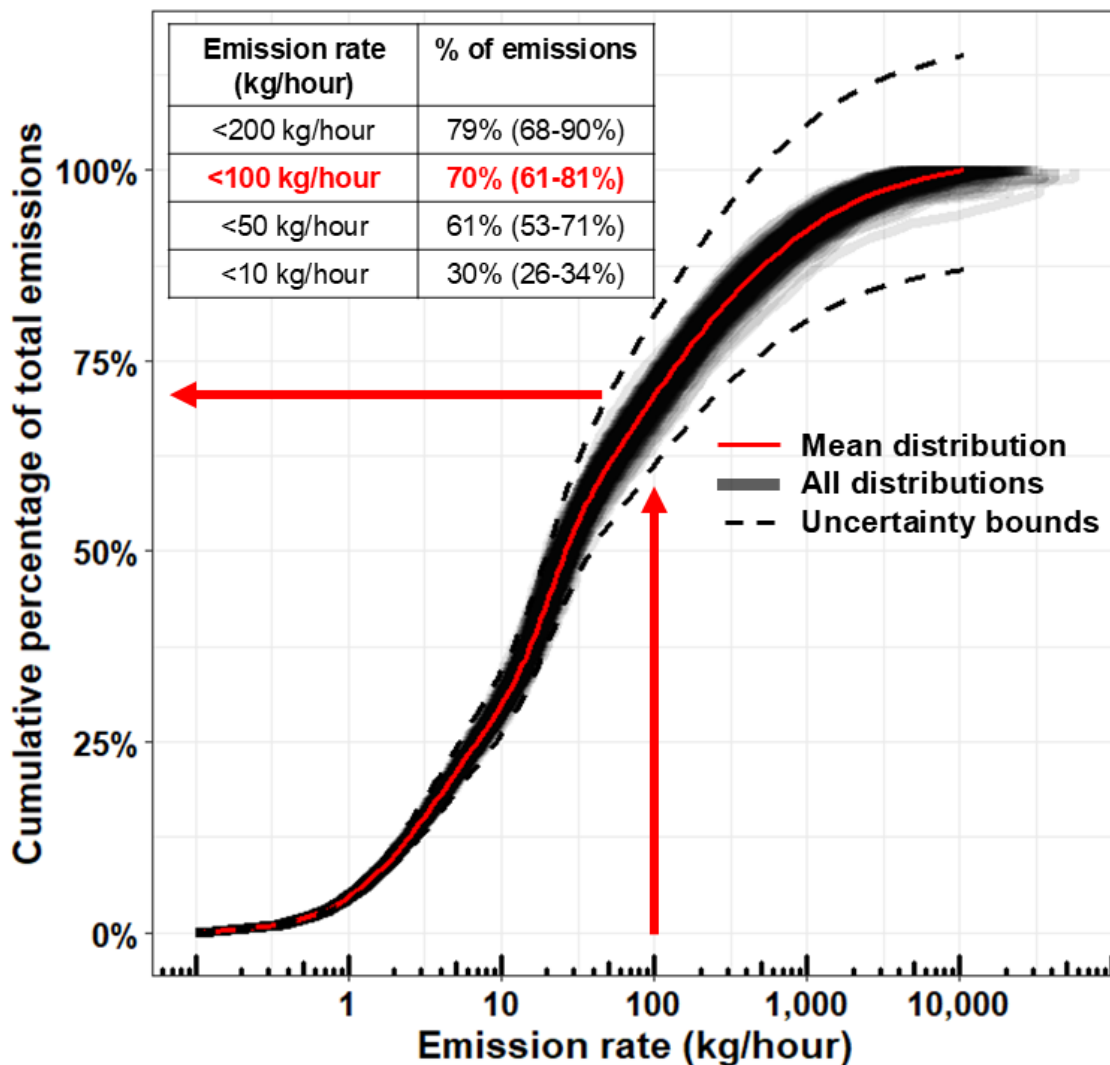
Figure 3: Results from 500 estimated facility-level emission distributions showing the cumulative percentages of
total methane emissions contributed from facilities emitting below methane emission rate thresholds. For example,
facilities emitting <100 kg/hr account for 70% (61-81%) of total methane emissions. The inset table in the upper left
displays the total percentage of methane emissions contributed from several discrete emission rate thresholds with
95% confidence intervals shown in parenthesis.

387

388   The distribution for our national-level methane emissions follows an S-shaped curve, noting that the x-axis

389   (i.e., facility-level methane emission rates) is presented in the $\log_{10}$ scale. From 0.1 to 1 kg/hr, we observe a plateau

390   in the distribution curve indicating that increasing emission rates within this range do not significantly increase the

391   percentage contribution to total regional emissions (Fig. 3), similar to the findings in Ravikumar et al. (2019). From 1

392   to 100 kg/hr, we see a sharper rise in the emission distribution, indicating that increasing emission rates at this range

393   lead to a more substantial contribution to total methane emissions, and account for 68% (60 – 75%) of total methane

emissions (Fig. 3, Table S4). Above an emission rate threshold of 100 kg/hr, we see an exponential decline in the percentage contributions of total emission with increasing emission rates, with total methane emissions in this range amounting to 28% (18 – 37%) of the total oil/gas emissions. Facilities emitting at the 1-10 kg/hr and 100-1,000 kg/hr ranges contribute a similar cumulative percentage at 26% (23 - 29%) and 22% (18 - 26%) respectively. Similar percentage contributions are also observed between the 0.1-1 kg/hr and >1,000 kg/hr ranges at 4.5% (4.0 - 5.1%) and 6.1% (2.6 - 13%) respectively. Overall, we find that the highest contribution to total national CONUS methane emissions occurs from facilities emitting in the 10-100 kg/hr range at 42% (37 - 46%). In terms of facility counts, from the 673,940 total active oil/gas facilities we estimate in the CONUS for 2021, we estimate that essentially all (i.e., ~99.9%) of these facilities emit methane below 100 kg/hr.

Our facility-level model estimates total methane emissions from US upstream/midstream oil/gas emissions for 2021 to be 14.6 (12.7 - 16.8) Tg/yr, or 1,668,000 (1,453,000 – 1,921,000) kg/hr (Fig. 4), which corresponds to a gross gas production normalized loss rate of 2.4%, assuming a uniform 80% methane content in natural gas across oil/gas producing regions in the CONUS. This national emission total of 14.6 (12.7 - 16.8) Tg/yr is more than double the EPA Greenhouse Gas Inventory Report for natural gas and petroleum systems in 2021, excluding post-meter and distribution methane emissions (Inventory of U.S. Greenhouse Gas Emissions and Sinks, 2024). We compare our total national estimates to previous estimates by seven studies that predominantly utilize satellite-based remote-sensing platforms such as GOSAT and TROPOMI inversions (Lu et al., 2022, 2023; Maasakkers et al., 2021; Shen et al., 2022; Worden et al., 2022) except for Alvarez et al. (2018) and Omara et al. (2024) who developed unique facility-based modeling approaches using empirical measurement data collected from multiple oil/gas basins in the CONUS (Fig. 4). Our estimate of national methane emissions overlaps with six out of seven other national estimates of oil/gas methane emissions for the US, with a combined average of 13.1 (ranging from 11.1 - 15.7) Tg/yr. We do not estimate methane emissions from gathering/transmission/distribution pipelines, post-meter emissions, abandoned oil and gas wells, and refineries due to the scarcity of measurement-based data for these sources. Total methane emissions from these sources emit ~2 Tg/year of methane emissions based on other studies (Williams et al., 2021; Alvarez et al., 2018; Omara et al., 2024; Weller et al., 2020; Inventory of U.S. Greenhouse Gas Emissions and Sinks, 2024). Overall, our total national estimate of CONUS methane emissions for 2021 shows

good agreement with multiple independent and recent measurement-based estimates.
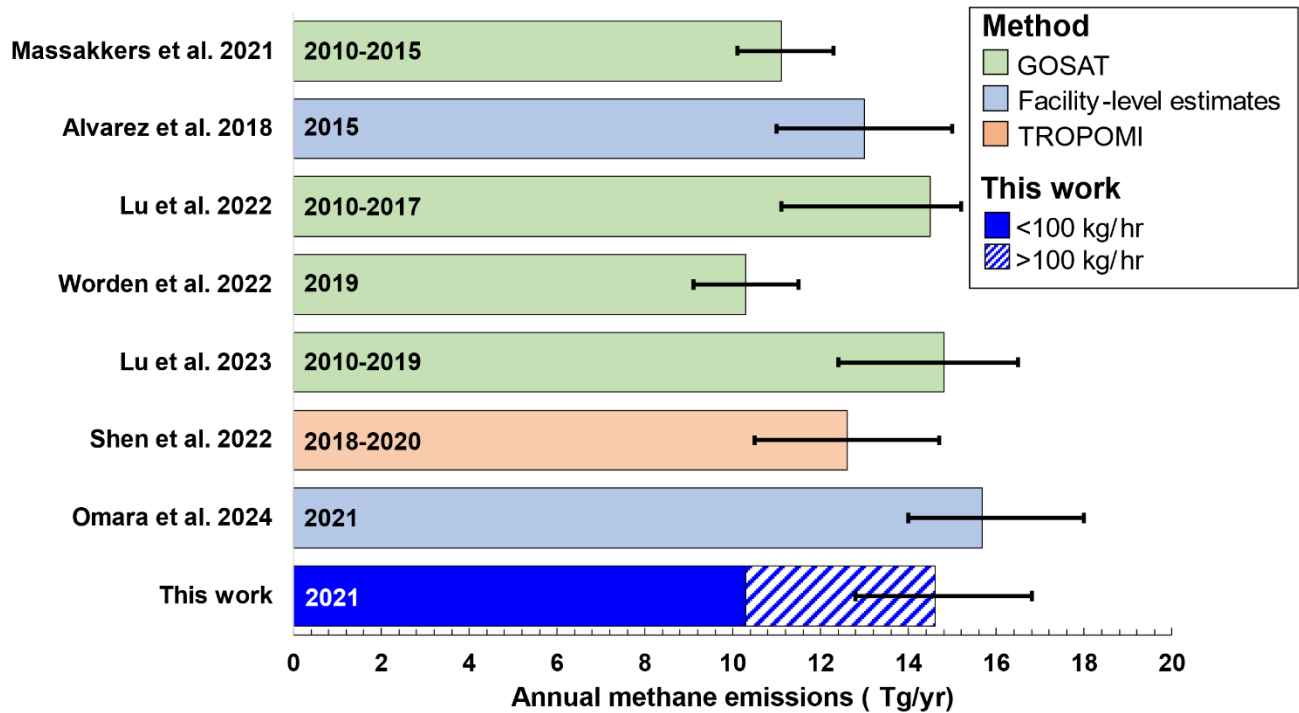
Figure 4: Comparison of total CONUS oil/gas emissions for 2021 from this facility-level measurement-based inventory compared to empirical estimates from other studies. Bars are colored according to the methodology used to derive the total national estimates, and the years within the bars represent the corresponding time periods for the estimates. Black inset lines represent 95% confidence intervals. Our total estimates for "This work" do not include emissions from other oil/gas methane sources such as abandoned oil and gas wells, transmission/gathering/distribution pipelines, post-meter emissions, and refineries. Emission estimates from Omara et al. (2024) do not include methane emissions from abandoned oil and gas wells. We assume that the remote sensing estimates (i.e., GOSAT and TROPOMI) include all oil/gas methane sources, including downstream emissions.

3.2 Distribution of emission rates at the basin-level scale

Among the top nine emitting oil/gas basins in the CONUS, we observe variations among the different basins in terms of the methane emission distributions, especially at higher emission rate thresholds (Fig. 5). The majority of the top nine emitting oil/gas basins in Fig. 5 show higher percentage contributions from facilities emitting <100 kg/hr when compared to our national estimate of 70% (61 – 81%) (Fig. 3). These percentage contributions vary from ~80% in the Permian, Appalachian, and Eagle Ford basins, up to ~90% in the oil-dominant San Joaquin basin. Only the Anadarko and Bakken basins have notably lower contributions to total emissions at the 100 kg/hr threshold at ~60% compared to the national level, which is still a significant majority of total methane emissions. Despite these variations, our facility-level model estimates that the majority of total national oil/gas emissions are consistently contributed from facilities emitting <100 kg/hr for the top nine emitting basins.

443   Our estimated facility-level emission distributions for the top nine emitting oil/gas basins all follow an S-

444   shaped curve (Fig. 5) like the national distribution (Fig. 3), albeit with certain variations. For all basins, the initial

445   plateau in the emissions distribution curves ends at around 1 kg/hr before beginning to rise more steeply. For the

446   Appalachian and San Joaquin basins, the second plateau is at the 20-50 kg/hr emission rate threshold (Fig. 5). For

447   the remaining basins, the rise in the emission distribution curves plateaus gradually, indicating a more consistent

448   relationship of emission rate thresholds to their contribution to total emissions. The variability displayed among the

449   500 basin-level simulations differs among the oil/gas basins, with less spread in the 500 estimated methane

450   emissions distributions for the Appalachian, Anadarko, and Permian basins compared to the Uinta, Denver-

451   Julesburg, and San Joaquin basins (Fig. 5 and Fig. S6). These variations are likely caused in part by the overall total

452   basin-level methane emissions, where an extremely high estimated methane emission rate would have a greater

453   impact on the percentage contribution to the total for basins with lower overall emissions (e.g., the apparent outliers

454   for the Greater Green River and Bakken basins in Fig. 5). We discuss below other plausible causes for basin-to-

455   basin variability in the estimated methane emission distributions.

456   In terms of total methane emissions, the top two emitting oil/gas basins are the Permian and Appalachian,

457   which collectively account for 5.2 (4.4 – 6.3) Tg/year (Fig. S1) or 37% of total upstream and midstream oil/gas

458   methane emissions. This exceeds the cumulative contribution from the other seven highest emitting oil/gas basins

459   which collectively account for 3.7 (2.9 – 5.0) Tg/yr. Notably, we find that the highest emissions in the CONUS

460   occur from regions outside of any basin boundary 4.3 (1.2 – 6.3) Tg/year. Our estimates for basin-level total

461   emissions also show good agreement with remote-sensing satellite-based observations (Fig. S1), except for the

462   Appalachian, Bakken, Greater Green River, and Denver-Julesburg basins where our results are consistently more

463   than double those from the remote-sensing studies that used a prior-emission based inversion result (Lu et al., 2023;

464   Shen et al., 2022). These four basins are in regions with relatively low TROPOMI observation counts and densities

465   compared to other regions in the CONUS (Shen et al., 2022), in addition to other factors that could influence

466   satellite-based inversions such as the presence of many non-oil/gas sources such as coal, livestock, and landfills.

467   Overall, our estimates of total basin-level emissions are consistent with satellite-based observations.

468

469

470
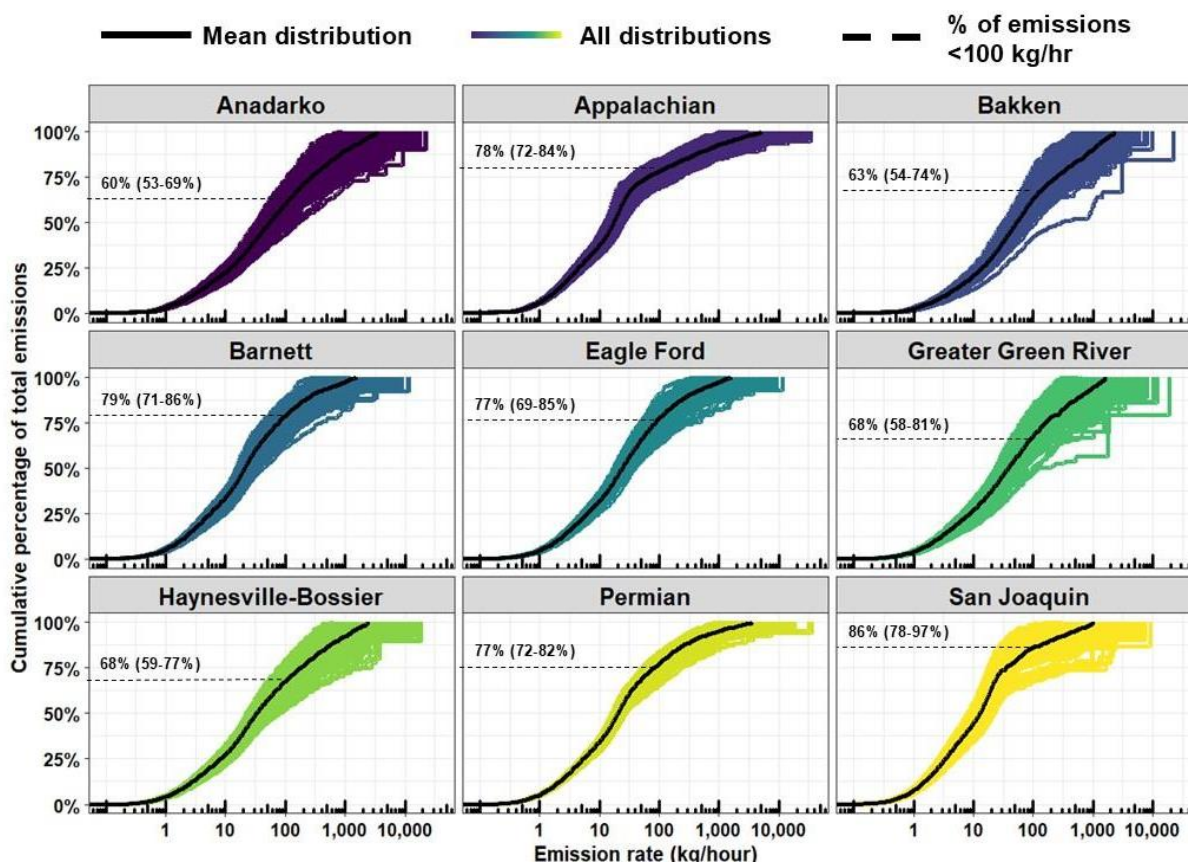
Figure 5: A) Results from 500 model simulations showing the cumulative methane emissions distribution curves for
total upstream/midstream oil/gas methane emissions for the top nine emitting oil/gas basins in the CONUS for 2021.
The model averages for each basin are shown in solid black lines. Inset dashed lines represent the percentage
contributions of total emission from sources emitting <100 kg/hr. Emission distribution curves for the remaining
eleven oil/gas basins in the CONUS are shown in Fig. S6, and a map of the spatial boundaries used for the different
oil/gas basins is shown in Fig. S10.

3.3 Distribution of emission rates by facility category

We find significant variations in the methane emission rate distribution curves among the different facility

categories (Fig. 6A). Over 50% of total methane emissions from low (i..e, <15 boe/day, or <0.13 kt of methane

production per year and non-low production well sites, lit flares, and G&B compressor stations occur from facilities

emitting <100 kg/hr (Fig. 6A). In contrast, only 17% (15-18%) of emissions from processing plants, 19% (18-20%)

of emissions from T&S compressor stations, and 9% (7-12%) of emissions from unlit flares are contributed from

emission sources <100 kg/hr. Similar variability is also observed at other emission rate thresholds, such as only 1%

(0-2%) of total emissions for T&S compressor stations, unlit flares, and processing plants originating from facilities

emitting at rates <10 kg/hr, compared to 50% (43-58%) from low producing well sites and 30% (24-35%) from non-

low producing well sites (Fig. 6A). At higher emission rate thresholds, we find that 33% (20-45%) of total emissions

from T&S compressors and processing plants are emitted from facilities <200 kg/hr, compared to 84% (68-93%)

490 from non-low producing well sites (>boe/day of combined oil and gas), 86% (83-88%) from VIIRS flare detections,

491 78% (70-86%) from G&B compressor stations, and essentially 100% of emissions from low producing well sites.

492 A breakdown of the 673,940 total facilities in our model has 541,970 as low-producing well sites, followed

493 by 121,824 non-low-production well sites, 4,431 G&B compressor stations 2,093 T&S compressor stations, 919

494 processing plants, and 3,153 total VIIRS flare detections. Of these 673,940 total facilities, 99.5% (99.4 – 99.6%)

495 emit methane at rates <100 kg/hr (Fig. S11), and in turn contribute 70% of total methane emissions (Fig. 3). Overall,

496 we estimate that 68% of total CONUS oil/gas methane emissions for 2021 come from production well sites, of

497 which 44% are from low-production well sites with combined oil/gas production <15 boe/day (i.e., <0.13 kt of

498 methane production per year), and the remaining 24% from non-low production well sites (i.e., >15 boe/day) (Fig.

499 6B). Midstream facilities contribute 29% of total methane emissions, with 13% from T&S compressors, 8% from

500 processing plants, 7% from G&B compressor stations. The remaining 4% from VIIRS flare detections are evenly

501 split with 2% each from lit and unlit flares respectively. Based on the population counts for each facility category

502 and their corresponding total methane emissions, the average methane emission rate per facility category is highest

503 for processing plants at 146 (115 – 283) kg/hr, followed by 106 (89 – 129) kg/hr for T&S compressor stations, 27

504 (25 - 29) kg/hr for G&B compressor stations, 3.3 (2.9 – 3.8) kg/hr for non-low producing well sites, and 1.3 (1.2 –

505 1.5) kg/hr for low producing well sites. For VIIRS flares detections, we find a large difference in average emissions

506 between lit flares at 11 (9.2 – 13) kg/hr and unlit flares at 205 (132 – 294) kg/hr.

507 Production well sites constitute the bulk of total methane emissions among the facility categories we

508 considered, with most of these emissions contributed from low production well sites. Overall, we find that 67-90%

509 of well site emissions originated from only 10% of national oil and gas production in 2021 (Fig. S7), highlighting a

510 disproportionately large fraction of emissions relative to production. In terms of individual well site level production

511 values, the same 67-90% of total cumulative methane emissions were contributed from well sites producing >50

512 boe/day (i.e., 0.43 kt of methane production per year) or lower. For well sites producing 15 boe/day (i.e., 0.13 kt of

513 methane production per year) or lower, which is the production threshold used to define a well site as being

514 marginally producing in previous work (Deighton et al., 2020; Omara et al., 2022), we find that these low producing

515 well sites accounted for 50-75% of total well site emissions, or 4.7-6.8 Tg/yr.

516

517

518
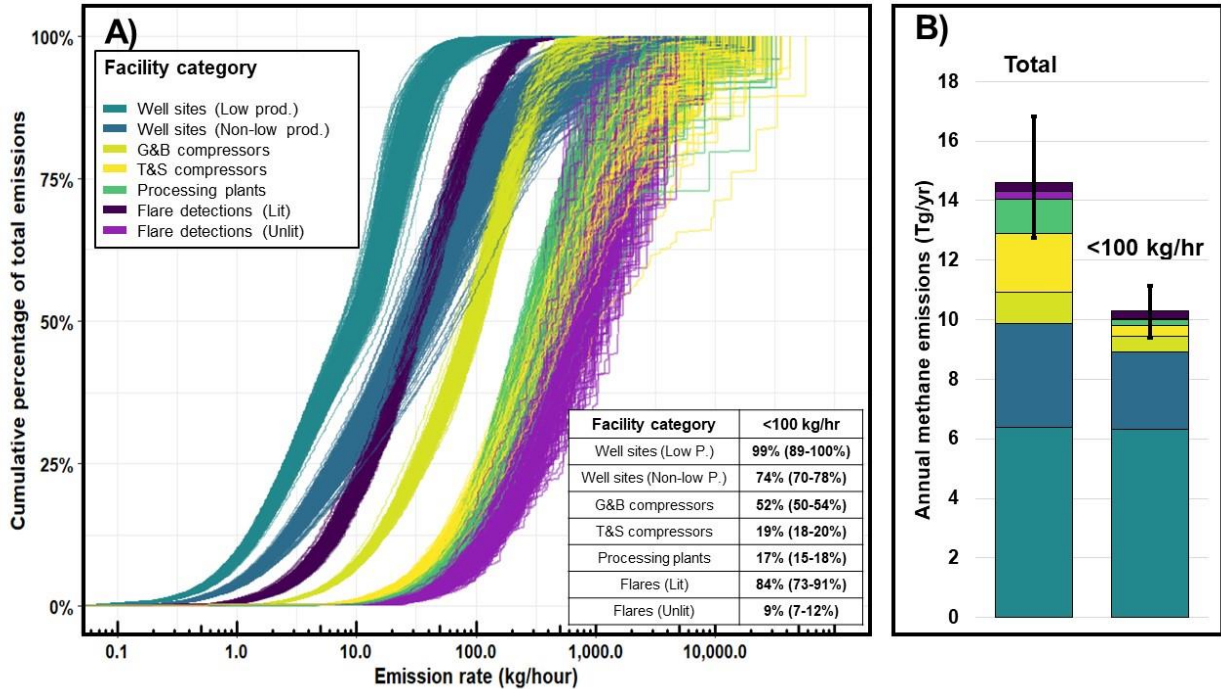
Figure 6: A) Results from an ensemble of 500 estimated methane emission distributions showing the percentage of
total methane emissions among facility categories contributed from facilities emitting at rates below an emission rate
threshold. The inset table on the bottom right displays the discrete percentage contributions to total methane
emissions contributed from facilities emitting <100 kg/hr. B) Breakdown of total annual methane emissions
contributed from all emitting facility categories and those emitting at rates <100 kg/hr.

524

3.4 Comparisons to aerial remote sensing studies

526

We perform comparisons of the percentage contributions of methane emissions from facilities emitting

below discrete emission rate thresholds between seven aerial remote sensing campaigns across four distinct regions

and our estimated facility-level results (Fig. 7). The aerial remote sensing technologies include data from Bridger

GML measurements (Kunkel et al., 2023; Xia et al., 2024), MethaneAIR (Omara et al. 2024; Miller et al. 2023), and

the results from Global Airborne Observatory and next-generation Airborne Visible/Infrared Imaging Spectrometer

campaigns (Cusworth et al., 2022) which are also included in the aerial detections used by Sherwin et al. (2024). In

comparing the percentage contributions to total emissions from low-emitting sources between our facility-level

estimates and the aerial remote sensing campaigns, we find that emission contributions agree well across aerial

remote sensing campaigns for the total percentage of methane emissions from facilities emitting, as seen in Fig. 7

for both less than 100 kg/hr and 200 kg/hr.

For the Bridger GML remote sensing campaigns (Kunkel et al., 2023; Xia et al., 2024), we find good

agreement in the percentage of total emissions contributed from facilities emitting <200 and <100 kg/hr compared to

our facility-level model estimates (Fig. 7). A comparison of continuous emissions distribution curves between our

540   facility-level emission distributions and two Bridger GML aerial remote sensing campaigns (Kunkel et al., 2023;

541   Xia et al., 2024) targeting four oil/gas basins is shown in Fig. S3. The Bridger GML aerial sampling platform has the

542   lowest LOD among the aerial campaigns we analyze in this work and a similar source resolution (i.e., 30 meters) to

543   our facility-level model (i.e., 50 meters), allowing for a more detailed comparison of continuous emission

544   distribution curves due to the higher number of detected methane sources at low emission rates provided by Bridger

545   GML surveys. We find close agreement between our facility-level methane emission distribution curves and the

546   observed emissions by Bridger GML in the four-basin aggregate provided by Xia et al. (2024) (Fig. S3A) which

547   includes Anadarko, Bakken, Eagle Ford and Permian basins (individual basin data are not currently available in Xia

548   et al. (2024)), as well as separately for the Permian remote sampling campaign (Fig. S3B) by Kunkel et al. (2023),

549   with the measured emissions from the Bridger GML surveys overlapping with our facility-level model simulations

550   throughout the continuous distribution of methane emission rates.

551   For the multiple aerial remote sensing campaigns performed by Cusworth et al. (2022), we generally find

552   good agreement with all of our estimates statistically overlapping for discrete emissions rate thresholds of <100

553   kg/hr and <200 kg/hr for the Permian and Uinta oil/gas basins (Fig. 7). For the San Joaquin and Denver-Julesburg

554   oil/gas basins, we see good agreement at the emission rate threshold of <200 kg/hr and at <100 kg/hr (i.e.

555   overlapping uncertainty bounds). For the Appalachian basin, we find broad agreement at both emission rate

556   thresholds of <100 kg/hr and <200 kg/hr, with our results consistently showing a 20-30% greater contribution from

557   emission sources below the discrete emission rate thresholds (Fig. 7). We find the closest agreement in the Permian

558   and Uinta oil/basins, where the differences in the average percentage contributions vary from -9% to +4% across the

559   three discrete emission rate thresholds of <100 and <200 kg/hr (Fig. 7). In Denver-Julesburg and Appalachian

560   basins, the differences are observed to be larger, compared to other basins, where the differences in average

561   percentage contributions across the discrete emission thresholds vary from -30% to +18%, however, they are within

562   our estimated uncertainty bounds. The detected point sources by Cusworth et al. (2022) in the Denver-Julesburg and

563   Appalachian basins contain many non-oil/gas point sources (Table S4), which may lead to additional uncertainty in

564   the comparisons for these basins since we use the relative proportions of point sources to subtract an estimated

565   contribution of non-oil/gas point sources from the TROPOMI estimates to provide a more direct comparison

566   between our estimates (since our study only focuses on upstream and midstream oil and gas sectors) and those of

567   Cusworth et al. (2022). Notably, the Appalachian basin contains the highest percentage contribution of non-oil/gas

568   point sources at 67% (Table S4). In contrast, we note that all of the detected point sources by Cusworth et al. (2022)

569   in the Permian and Uinta basins were attributed to oil/gas point sources (Table S4).

570   Our comparisons to the available flight results from MethaneAIR, which quantifies both total regional

571   methane emissions and high-emitting point sources >200 kg/hr from the same aerial platform (Chulakadabba et al.,

572   2023), show close agreement between our facility-level estimates and the available aerial campaigns in the Uinta

573   and Permian basins for facilities emitting <200 kg/hr (Fig. 7B). For the MethaneAIR flight in the Uinta basin, we

574   estimate that 92% (46 - 100%) of total oil/gas methane emissions are from sources emitting <200 kg/hr, compared to

575   88% from MethaneAIR (Fig. 7B). For the available flight in the Permian basin from MethaneAIR, we estimate total

576   contributions from sources emitting <200 kg/hr at 77% (59 – 90%) compared to the 71% estimated by MethaneAIR

577   (Fig. 7B).

578   Overall, our findings show that our facility-level estimates closely agree with the results from multiple

579   aerial remote sensing campaigns from different regions and using various measurement methods.

580
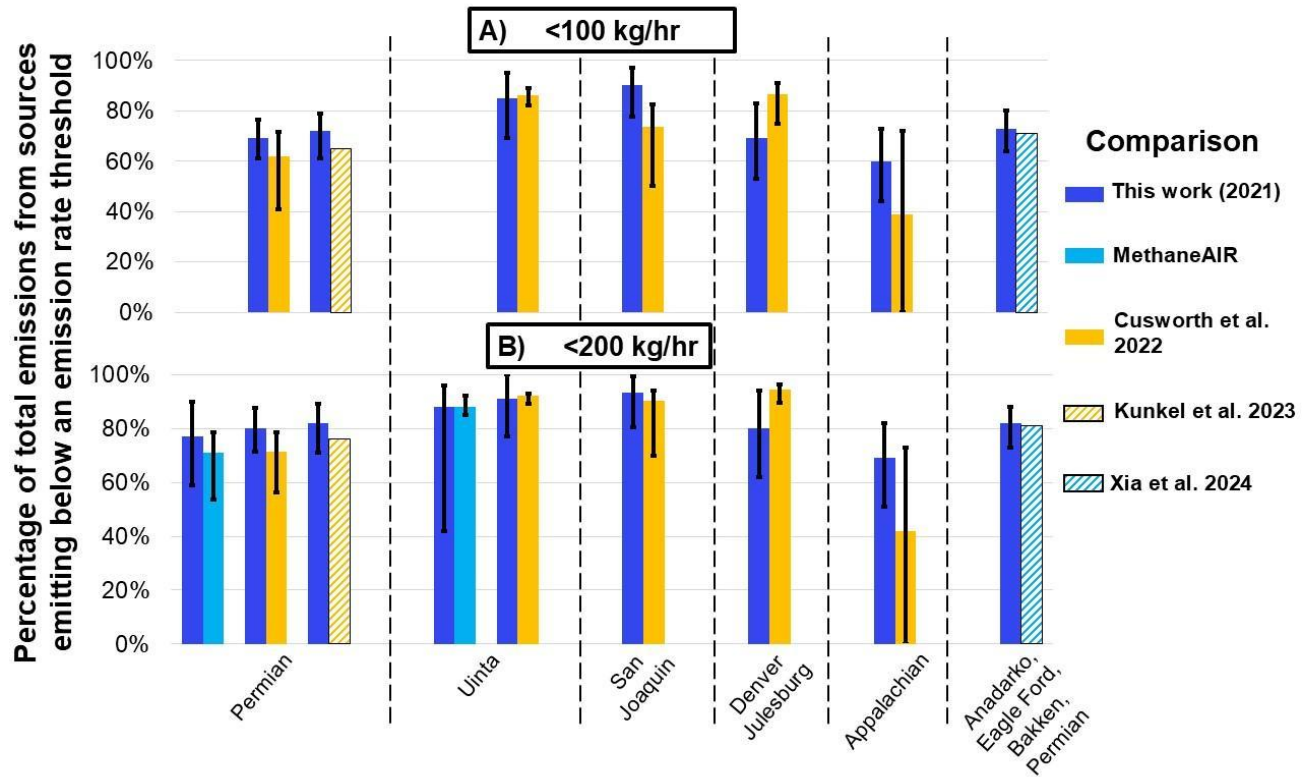
581

582   **Figure 7:** Comparisons of the cumulative percentage of oil/gas methane emissions from all oil/gas facilities emitting
583   A) <100 kg/hr, and B) <200 kg/hr, between our facility-level empirical emissions estimates and aerial remote
584   sensing campaigns. Bars are colored according to the study and grouped according to the target oil/gas basin(s). All
585   results from the facility-level simulations (i.e., this work) are constrained to the spatial boundaries of the aerial
586   campaigns for direct comparisons (note that for a given basin, spatial boundaries might be slightly different).
587   Uncertainty bars for the facility-level simulations are the 2.5th and 97.5th percentiles of 500 simulations. Maps of all
588   spatial boundaries used for comparisons are provided in Fig. S2. Comparisons to MethaneAIR are not performed at
589   the <100 kg/hr threshold because MethaneAIR detections are not available for point sources below this emission
590   rate threshold.

591

592   **4 Discussion**
593

594   Understanding how facilities with different magnitudes of emissions contribute to total regional emissions

595   has direct policy implications for methane quantification and mitigation, such as the selection of

596   measurement/screening methods with the appropriate detection sensitivities (Ravikumar et al., 2018). Our main

597   finding is that 70% of total oil/gas methane emissions from the upstream/midstream sectors come from facilities

598   emitting at rates <100 kg/hr, which is the emission rate threshold above which point source emissions are referred

599   to as "super-emitting" oil/gas source by the EPA (Standards of Performance for New, Reconstructed, and Modified

600   Sources and Emissions Guidelines for Existing Sources: Oil and Natural Gas Sector Climate Review, 2024). While

601   detecting and mitigating emissions from super emitters are important (Cusworth et al., 2022; Duren et al., 2019;

602   Sherwin et al., 2024), our results underscore the need to account for oil/gas methane sources emitting at lower rates,

603   as the cumulative contribution of lower-emitting sites accounts for a large majority of emissions across US oil/gas

604   basins. Facility-level, measurement-based data collected in other countries present a similar story. From a sample of

605   sites (n=302) measured via Bridger GML remote sensing platform in British Columbia, Canada (Tyner and Johnson,

606   2021), roughly 60% of the total quantified oil/gas site-level emissions originate from sites emitting <32 kg/hr. In

607   Romania, a site-level measurement-based inventory (Stavropoulou et al., 2023) using 178 measurements finds that

608   oil production facilities emitting <100 kg/hr contribute 78% of total oil/gas methane emissions in the studied region.

609   In short, the high percentage contribution from lower-emitting (<100 kg/hr) oil/gas facilities that account for a large

610   majority of total emissions is not unique to the US and is likely present in other countries as well. A combination of

611   approaches that characterize entire emission distributions across populations of sites (i.e., not just focusing on

612   measuring super-emitters) and quantification of regional-level emissions is needed in other countries to quantify the

613   relative contributions of low-emitting sources that in aggregate can be significant sources of overall oil/gas methane

614   emissions. Most of our analysis centers around quantifying the percentage contributions of oil/gas methane sources

615   emitting below one discrete emission rate threshold (i.e., <100 kg/hr, per EPA's definition of a super-emitter). We

616   estimate that over 99% of the total oil/gas facilities that we analyze in this work emit below 100 kg/hr (Fig. S11),

617   which in turn contribute 70% (61 – 81%) of total methane emissions (Fig. 3). The emission rate threshold of 100

618   kg/hr is relevant to US policy decisions (EPA's Final Rule for Oil and Natural Gas Operations Will Sharply Reduce

619   Methane and Other Harmful Pollution., 2024), but we also illustrate the importance of a complete characterization of

620   emissions, which gains importance as newer methane monitoring technologies have different LODs. For example,

621   the effective LOD at high probabilities of detection for available point source imaging satellites of ~200 kg/hr

622   (Jacob et al., 2022) would only be able to quantify 21% (10-32%) of all oil/gas point sources in the CONUS, if the

623   full oil/gas sector was mapped in its entirety, based on our facility-level results. When considering the relationship

624   of facility-level emission rates to total cumulative methane emissions, we find that oil/gas methane emissions in the

625   CONUS are dominated by many low-emitting facilities, which relates directly to methane measurement

626   technologies.

627   Point source-focused remote sensing platforms offer the advantage of rapidly surveying large areas (i.e.,

628   100's-1,000's km^2) which facilitates the detection and quantification of high-emitting point sources (Cusworth et al.,

629   2022; Duren et al., 2019; Sherwin et al., 2024). In contrast, logistical constraints often limit the sample sizes for

630   ground-based vehicle sampling platforms, however, these limitations can be overcome with stratified random,

631 representative sampling and statistical analysis approaches like this work. Ground-based measurement platforms
632 provide much lower LODs (i.e., <1 kg/hr) when compared to remote sensing platforms, which are necessary to
633 quantify emissions from the large number of small methane sources we find that contribute roughly three-quarters of
634 total regional oil/gas emissions in the CONUS and will only improve as additional ground-based measurements are
635 gathered. Overall, our main findings highlight the importance of methods that can rapidly locate the small number of
636 high-emitting point sources we estimate, but our findings emphasize the need to account for the disproportionately
637 large majority percentage of total regional oil/gas emissions that are emitted from smaller diffuse methane sources.

638 When extrapolating our facility-level model results to the basin-level we see variations among the emission
639 distribution curves for different oil/gas basins, but still find that most methane emissions come from facilities
640 emitting <100 kg/hr. The variations in the emission distribution curves for different basins are driven by many
641 factors, such as the: production characteristics, number and density of facilities, different types and relative counts of
642 facility categories, the availability of empirical measurement data used to model emissions, and the total oil/gas
643 methane emissions (i.e., the denominator). For example, the Appalachian basin is dominated by a high number of
644 older low-production well sites (Deighton et al., 2020; Riddick et al., 2019; Enverus, 2024) with fewer midstream
645 facilities such as processing plants and G&B compressors, which contrasts with the Bakken basin where we find a
646 high number of midstream facilities, high-producing well sites, and VIIRS flare detections (Elvidge et al., 2015;
647 Enverus, 2024). When comparing the emissions distribution curves for the Bakken and Appalachian basins (Fig. 5),
648 we observe higher contributions from lower-emitting facilities for the Appalachian compared to the Bakken. An
649 example of differences in basin-level production is shown in Fig. S4 and Fig. S5, where we see variable profiles
650 among the different oil and gas-producing basins in terms of well site production characteristics, which are the main
651 source of total methane emissions in this work (Fig. 6). We also observe the influence of total basin-level emissions
652 on the variability among our emission distribution curves, where large emitting sources in the San Joaquin basin can
653 lead to high variability among the estimated emission distribution curves compared to the Permian basin which has
654 roughly ten times the total emissions compared to the San Joaquin (Fig. 5). We note that a direct comparison of our
655 model results with aerial remote sensing methods may be limited, in part, by methodological differences in methane
656 quantification approaches (and underlying uncertainties). The remote sensing observations assessed here as
657 snapshots may capture facility-level emission distributions that are not well represented in annually averaged
658 methane emissions distributions, as we estimate here. Nevertheless, we find broad agreement with these independent
659 aerial remote sensing estimates at the basin scale and across smaller spatial domains, as discussed. Ultimately, as
660 many characteristics will influence methane emissions distribution curves among different oil/gas producing regions
661 in the CONUS, mitigation strategies will need to be structured accordingly to the region they are targeting.

662 Our results find that over half of cumulative methane emissions from three different facility categories
663 come from facilities emitting <100 kg/hr, including methane emissions from lit and unlit flares. We show how the
664 large contributions from small methane sources to total regional emissions are not unique to any one facility
665 category, but it is important to contextualize our emission distribution curves with the corresponding total regional
666 emissions. Our facility-level estimates find that the main source of oil/gas methane emissions in the CONUS are

667   oil/gas production well sites, of which the low production category is responsible for 44% (39 – 49%) of the total

668   estimated oil/gas methane emissions in the CONUS in 2021. Low-producing well sites, also known as "marginal

669   wells", have been shown in previous work to be a significant source of methane emissions, especially relative to

670   their contribution to overall oil/gas production (Deighton et al., 2020; Omara et al., 2022). Omara et al. (2022) found

671   that marginal wells contributed anywhere from 37%-75% of total methane emissions from production well sites,

672   which is like our estimates (i.e., 50-75%). Despite low production well sites having a lower mean emission rate

673   compared to other facility categories, the large facility counts result in significant aggregate total emissions of

674   methane. This implies that detection and mitigation strategies to reduce methane emissions from these and other

675   low-emitting oil and gas infrastructure (e.g., abandoned oil/gas wells) would require alternative mitigation and

676   detection approaches compared to those for the small number of super-emitting emission sources. For detection,

677   measurement methods that can measure emission rates between 0.1-100 kg/hr are required, since this range makes

678   up 70% of total methane emissions (Figure 3 and Table S1) as modeled herein. In terms of methane mitigation

679   policy, financial incentives, like the USD 4.7 billion from the Biden Bipartisan Infrastructure Law for abandoned

680   wells, could be used to prioritize the repair of old and leak-prone production well sites, as these low-producing well

681   sites only account for a small fraction (i.e., 5.6% in 2019) of total oil/gas production (Omara et al., 2022).

682   We see good agreement between our facility-level results and a majority of aerial remote sensing studies, which

683   are expected to capture a wide range of high-emitting facilities in a survey region. For example, when comparing

684   our model results to Kunkel et al. (2023) and Xia et al. (2024) we find that our estimated methane emissions closely

685   match the distribution of methane emissions measured in Bridger GML surveys (Fig. S3). We also find good

686   agreement to satellite remote sensing estimates of emissions, such as our basin-level (Fig. S1) and national-level

687   comparison to satellite inversions (Fig. 3), and other aerial remote sensing study regions (Table S2). Our

688   comparisons of the contributions of low-emitting sources below discrete emission rate thresholds also agree closely

689   with recent MethaneAIR, Kairos Aerospace, GAO, and AVIRIS-NG aerial surveys, whose results also highlight the

690   importance of small methane sources to overall oil/gas methane emissions. Recently, Sherwin et al. (2024)

691   suggested that a majority of total emissions originate from a small fraction of high-emitting sites. Notably, most of

692   the aerial measurements that are used in Sherwin et al. (2024) are obtained from the Cusworth et al. (2022) study,

693   with which we see good agreement (Fig. 7). Sherwin et al. (2024) perform an alternative analysis than Cusworth et

694   al. (2022) for aerially measured sources with <3 overpasses and assume that sources with one or two overpasses

695   emit at their observed intermittency of 100%, 50%, or 0% of the time. This difference in analytical approaches

696   produces higher contributions from aerial emissions in Sherwin et al. (2024) by 31% on average for seven aerial

697   campaigns compared to Cusworth et al. (2022) (Table S7), which uses a resampling approach described earlier in

698   the Methods Section 2.4. In addition, emissions from Sherwin et al. (2024) that are below aerial detection limits are

699   estimated using a combination of an equipment-level bottom-up model presented in Rutherford et al. (2021) for

700   production well sites, and emission factors from the U.S. Greenhouse Gas Inventory (Inventory of U.S. Greenhouse

701   Gas Emissions and Sinks, 2024) for midstream facilities, which produces 52% lower emissions on average for seven

702   aerial campaigns (Table S7). Therefore, the aerially measured emissions in Sherwin et al. (2024) are higher and the

703   emissions below aerial detection limits are lower which leads to a higher contribution to total methane emissions

704 from high-emitting facilities (Table S7). Ultimately, the broad agreement we find across multiple disparate

705 measurement techniques and platforms across Bridger GML aerial campaigns (Kunkel et al., 2023; Xia et al., 2024),

706 MethaneAIR measurements (MethaneAIR L4 Area Sources 2021 | Earth Engine Data Catalog, 2024; Omara et al.,

707 2024), and the multiple surveyed regions presented in Cusworth et al. (2022), altogether provide collective evidence

708 about the large contribution of smaller emission sources to total regional emissions.

709 Given the variability in methane detection technologies, a range of approaches can be taken to estimate methane

710 emission rate distributions, each providing unique advantages and disadvantages. MethaneAIR provides a novel

711 remote sensing approach where high-emitting point sources, distributed area sources and total regional emissions are

712 quantified using the same aerial platform, providing the ability to directly measure high-emitting point source and

713 diffuse area contributions to total regional estimates. In the work by Xia et al. (2024) they combine measurements

714 from Bridger GML across four oil/gas basins and use component-level simulations to account for facilities emitting

715 below the 3 kg/hr LOD of Bridger GML. Other approaches also exist, such as Cusworth et al. (2022) who combine

716 TROPOMI inversions to estimate total regional methane emissions with point source emissions quantified from their

717 aerial detection platforms (i.e., GAO, AVIRIS-NG). Similarly, Sherwin et al. (2024) combine point source emissions

718 measured via aerial remote sensing with site/facility-level emission rates estimates calculated from a combination of

719 an equipment-level bottom-up model for production well sites (Rutherford et al., 2021) and emission factors from the

720 2023 GHGI for midstream facilities (Inventory of U.S. Greenhouse Gas Emissions and Sinks, 2024) for facilities

721 emitting below aerial detection limits. Remote sensing studies have key advantages over ground-based sampling

722 platforms, such as rapidly surveying wide areas and capturing higher-emitting point sources, but have variable LODs

723 depending on the target region, topography, measurement technology, presence of co-located non-oil/gas methane

724 sources (i.e., source attribution), weather conditions, infrastructure density, and infrastructure type(s). These variables

725 pose additional challenges when quantifying the contributions from facilities emitting above/below specific emission

726 rate thresholds, which are critical information to inform mitigation policy. Assessing performance, tracking mitigation,

727 and accurate reporting requires building a comprehensive picture of emissions by characterizing all emitters big and

728 small, and reconciling with total basin/sub-basin level emissions. Ultimately, the key seems to be merging the best

729 data from both approaches to build a hybrid inventory, ideally using a multi-tiered system with multiple methods that

730 span a range of LODs that allow for gathering empirical measurements from facilities emitting at all parts of the

731 methane emission distribution curve. Our study is a step in that direction considering measurement-based data while

732 presenting a robust comparison with available independent remote sensing measurements. At the same time, large-

733 area aggregate emissions data obtained from wide-area remote sensing mapping or mass balance surveys can better

734 constrain total regional emissions (e.g. Cusworth et al. 2022; Omara et al. 2024) towards a more empirically robust

735 denominator in characterizing the relative contributions of small emission and high emission sources to total

736 emissions.

737 We show that our facility-level emission models produce national- and basin-level methane emissions estimates

738 that are in good agreement with other independent measurement-based studies. However, we note the following

739 limitations/biases that could be improved with future data collection efforts. The empirical measurements that we

use in our model are representative of the year and time they were measured (i.e., 2010-2020), meaning that they would not reflect any updates in regulatory practices or changes in facility operational and emission management practices. In addition, there are variations in the number of production well site empirical measurements among oil/gas basins (Table S3) although a sensitivity analysis shows that excluding data from individual oil/gas basins does not significantly impact our results (Fig. S9). Furthermore, there are several oil/gas methane emission sources that we do not account for in our estimates, which include: gathering/transmission/distribution pipelines, oil refining and transportation, abandoned oil/gas wells, offshore oil/gas infrastructure, post-meter sources, and oil/gas distribution infrastructure in urban areas. For some sources omitted in this work such as abandoned oil/gas wells, their inclusion would likely lead to a higher contribution from low-emitting facilities, since the highest recorded emission rate from an abandoned oil/gas well is 76 kg/hr (Riddick et al., 2024). For others such as oil refineries, their inclusion would likely lead to a lower contribution from small methane sources given their low facility counts and high per-site emissions (Duren et al., 2019). Despite their omissions, total methane emissions from these sources are currently estimated to account for 5-10% (Alvarez et al., 2018; Riddick et al., 2024; Inventory of U.S. Greenhouse Gas Emissions and Sinks, 2024; Williams et al., 2021) of total oil/gas sectoral emissions. Our estimates also utilize empirically measured emission rates from ground-based sampling platforms which are limited in number, especially in the case of processing plants (n=20) and T&S compressor stations (n=50) (Table S2). The empirical data used in our analysis includes a smaller sample of super-emitting facilities relative to those captured by remote sensing platforms (Duren et al., 2019; Sherwin et al., 2024), but our use of production-normalized loss rates and lognormal distributions to estimate facility-level methane emission rates anticipates and accounts for the possibility of finding low-probability, high-magnitude emissions that occur at rates beyond those that appear in our dataset of empirical observations. For example, our highest empirical emission rate is 1,360 kg/hr for a T&S compressor station, whereas our maximum estimated facility-level emission rate across all 500 facility-level emission distribution curves averages 7,500 kg/hr (3,000 - 21,000 kg/hr). Finally, we include a small number (i.e., 5% of total empirical data used in the model) of measurements for production well-sites gathered using ground-based component/source-level sampling methods from two studies (Deighton et al., 2020; Riddick et al., 2019). All measurements from these two studies targeted the lowest production cohort of production well sites and exhibited statistically lower emission rates than those gathered using facility-level ground-based methods for the same well site production cohort, meaning that any bias introduced by the inclusion of these measurements would lead towards the underestimation of total emissions and/or the percentage contributions from low-emitting sources. Despite these limitations, we have shown that our results are broadly in agreement with satellite- and aerial-based remote sensing studies at national/basin/local scales, and other facility-level estimates.

Going forward, several approaches can be used to better understand the percentage contributions from facilities emitting at different leak rate thresholds, and ultimately improve our understanding of oil/gas methane emissions in the CONUS and around the world. A combination of multiple satellite and aerial remote sensing approaches and synthesis of their data by bringing in point source detections at multiple thresholds at the same time characterizing total regional emissions as demonstrated using a compilation of multi-scale measurements seems a viable pathway towards building a more complete picture of the overall methane emissions. Combining aerial and satellite remote

777 sensing measurements with ground-based site/facility-level estimates presents itself as an effective next step, as
778 implemented/suggested by prior studies (Allen, 2014; Alvarez et al., 2018). Aerial or satellite remote sensing
779 platforms focused on point source detection offer the ability to rapidly locate the small number of the highest
780 emitting facilities that contribute a disproportionate fraction of emissions, offering valuable data on specific facility
781 locations that allow for rapid mitigation. However, more direct observational approaches are needed to acquire total
782 emissions data which according to this study is dominated by small-emitting sources that are undetected by high-
783 emitting point source detection systems. Facility-level population-based approaches can account for the lower-
784 emitting facilities that contribute the most total oil/gas methane emissions, which is needed for accurate emission
785 reporting and understanding the contributions of total emissions above/below emission rate thresholds. The ground-
786 based estimates can be further constrained by large-area aggregated emission quantification provided by regional
787 remote sensing or mass balance mapping approaches (Shen et al., 2022; Omara et al., 2024; Jacob et al., 2022)
788 towards producing a more robust overall emission quantification.

789 **5 Conclusions**

790 In conclusion, our work highlights several key aspects of oil/gas methane emission rate distribution curves
791 in the CONUS for 2021, which include:

792 1. A large majority (70%) of total national continental oil/gas methane emissions in the US originate from
793   lower-emitting facilities (<100 kg/hr).

794 2. Emission rate distributions vary among different oil/gas basins, but among the top nine producing basins
795   we consistently find that most methane emissions (60%-86%) originate from oil/gas facilities emitting at
796   rates <100 kg/hr.

797 3. Production well sites were found to be responsible for 70% of regional oil/gas methane emissions, from
798   which the sites that accounted for only 10% of national oil and gas production in 2021, disproportionately
799   accounted for 67-90% of the total well site emissions.

800 4. Our results were consistently found to be in close agreement with those from independent aerial/satellite
801   remote sensing estimates, both in comparing contributions from discrete emission rate thresholds and
802   continuous emissions distribution curves, which emphasize the importance of the large majority
803   contribution of small-emitting methane sources to total oil/gas methane emissions.

804 Our results highlight, and quantify, the significant contributions of the large number of low-emitting oil/gas
805 facilities to total regional/basin/local oil/gas methane emissions in the CONUS for 2021. In addition to the CONUS,
806 the small oil/gas methane sources are likely a significant component of total regional emissions in other countries as
807 well as recent data suggest from Romania and Canada (Stavropoulou et al., 2023; Tyner and Johnson, 2021) and
808 would need to be further investigated to build a comprehensive assessment of small-emitting methane emissions and
809 their relative contributions to total oil/gas methane emissions globally. This work emphasizes the need for multi-

810 scale approaches to quantify total regional oil/gas methane emissions; and at the same time characterize and account

811 for the large contribution from small emission sources dispersed across a wide area, in addition to incorporating data

812 on high-emitting point sources towards producing overall robust methane emission quantification.

813

814 **Data availability**

815 All 500 full emission rate distributions at the national level are available to download from Zenodo (link:

816 https://doi.org/10.5281/zenodo.13314532). All estimated methane emission rate distributions at the basin or small

817 target scale are available upon request. Empirical measurement data used in the estimation of the methane emission

818 distribution curves are available from the references listed in Table S2.

819

820 **Code availability**

821 R code used to create the methane emission distribution curves and figures is available upon reasonable request.

822

823 **Acknowledgements**

824 We acknowledge funding support from the Bezos Earth Fund. We would like to thank Jack Warren for his valuable

825 efforts in analyzing point source emissions from MethaneAIR aerial campaigns.

826

827 **Author contributions**

828 JPW and RG designed this study. JPW created the code used to produce all results, with inputs from MO, KM, DZA,

829 and AH. MethaneAIR analysis was provided by JB, MS, and SW. Multi-sensor airborne intercomparison was

830 performed by JPW and RG. JPW prepared the manuscript with input from all co-authors.

831

832 **Competing interests**

833 The authors declare that they have no conflict of interest.

834

835 **References**

836 Allen, D. T.: Methane emissions from natural gas production and use: reconciling bottom-up and top-down
837 measurements, Current Opinion in Chemical Engineering, 5, 78–83, https://doi.org/10.1016/j.coche.2014.05.004,
838 2014.

839 Alvarez, R. A., Zavala-Araiza, D., Lyon, D. R., Allen, D. T., Barkley, Z. R., Brandt, A. R., Davis, K. J., Herndon, S.
840 C., Jacob, D. J., Karion, A., Kort, E. A., Lamb, B. K., Lauvaux, T., Maasakkers, J. D., Marchese, A. J., Omara, M.,
841 Pacala, S. W., Peischl, J., Robinson, A. L., Shepson, P. B., Sweeney, C., Townsend-Small, A., Wofsy, S. C., and
842 Hamburg, S. P.: Assessment of methane emissions from the U.S. oil and gas supply chain, Science, 361, 186–188,
843 https://doi.org/10.1126/science.aar7204, 2018.

Enverus | Creating the future of energy together.: https://www.enverus.com/, last access: 25 March 2024.

Standards of Performance for New, Reconstructed, and Modified Sources and Emissions Guidelines for Existing Sources: Oil and Natural Gas Sector Climate Review: https://www.federalregister.gov/documents/2024/03/08/2024-00366/standards-of-performance-for-new-reconstructed-and-modified-sources-and-emissions-guidelines-for, last access: 22 July 2024.

AR6 Synthesis Report: Climate Change 2023: https://www.ipcc.ch/report/ar6/syr/, last access: 6 March 2024.

MethaneAIR L4 Area Sources 2021 | Earth Engine Data Catalog: https://developers.google.com/earth-engine/datasets/catalog/EDF_MethaneSAT_MethaneAIR_methaneair-L4area-2021, last access: 27 March 2024.

Brandt, A. R., Heath, G. A., and Cooley, D.: Methane Leaks from Natural Gas Systems Follow Extreme Distributions, Environ. Sci. Technol., 50, 12512–12520, https://doi.org/10.1021/acs.est.6b04303, 2016.

Brantley, H. L., Thoma, E. D., Squier, W. C., Guven, B. B., and Lyon, D.: Assessment of Methane Emissions from Oil and Gas Production Pads using Mobile Measurements, Environ. Sci. Technol., 48, 14508–14515, https://doi.org/10.1021/es503070q, 2014.

Caulton, D. R., Lu, J. M., Lane, H. M., Buchholz, B., Fitts, J. P., Golston, L. M., Guo, X., Li, Q., McSpiritt, J., Pan, D., Wendt, L., Bou-Zeid, E., and Zondlo, M. A.: Importance of Superemitter Natural Gas Well Pads in the Marcellus Shale, Environ. Sci. Technol., 53, 4747–4754, https://doi.org/10.1021/acs.est.8b06965, 2019.

Chan Miller, C., Roche, S., Wilzewski, J. S., Liu, X., Chance, K., Souri, A. H., Conway, E., Luo, B., Samra, J., Hawthorne, J., Sun, K., Staebell, C., Chulakadabba, A., Sargent, M., Benmergui, J. S., Franklin, J. E., Daube, B. C., Li, Y., Laughner, J. L., Baier, B. C., Gautam, R., Omara, M., and Wofsy, S. C.: Methane retrieval from MethaneAIR using the CO_2 Proxy Approach: A demonstration for the upcoming MethaneSAT mission, EGUsphere, 1–40, https://doi.org/10.5194/egusphere-2023-1962, 2023.

Chen, Y., Sherwin, E. D., Berman, E. S. F., Jones, B. B., Gordon, M. P., Wetherley, E. B., Kort, E. A., and Brandt, A. R.: Quantifying Regional Methane Emissions in the New Mexico Permian Basin with a Comprehensive Aerial Survey, Environ. Sci. Technol., 56, 4317–4323, https://doi.org/10.1021/acs.est.1c06458, 2022.

Chen, Y., Sherwin, E. D., Wetherley, E. B., Yakovlev, P. V., Berman, E. S. F., Jones, B. B., Hmiel, B., Lyon, D. R., Duren, R., Cusworth, D. H., and Brandt, A. R.: Reconciling ultra-emitter detections from two aerial hyperspectral imaging surveys in the Permian Basin, 2024.

Chulakadabba, A., Sargent, M., Lauvaux, T., Benmergui, J. S., Franklin, J. E., Chan Miller, C., Wilzewski, J. S., Roche, S., Conway, E., Souri, A. H., Sun, K., Luo, B., Hawthrone, J., Samra, J., Daube, B. C., Liu, X., Chance, K., Li, Y., Gautam, R., Omara, M., Rutherford, J. S., Sherwin, E. D., Brandt, A., and Wofsy, S. C.: Methane point source quantification using MethaneAIR: a new airborne imaging spectrometer, Atmospheric Measurement Techniques, 16, 5771–5785, https://doi.org/10.5194/amt-16-5771-2023, 2023.

Cusworth, D. H., Thorpe, A. K., Ayasse, A. K., Stepp, D., Heckler, J., Asner, G. P., Miller, C. E., Yadav, V., Chapman, J. W., Eastwood, M. L., Green, R. O., Hmiel, B., Lyon, D. R., and Duren, R. M.: Strong methane point sources contribute a disproportionate fraction of total emissions across multiple basins in the United States, Proceedings of the National Academy of Sciences, 119, e2202338119, https://doi.org/10.1073/pnas.2202338119, 2022.

Deighton, J. A., Townsend-Small, A., Sturmer, S. J., Hoschouer, J., and Heldman, L.: Measurements show that marginal wells are a disproportionate source of methane relative to production, Journal of the Air & Waste Management Association, 70, 1030–1042, https://doi.org/10.1080/10962247.2020.1808115, 2020.

Duren, R. M., Thorpe, A. K., Foster, K. T., Rafiq, T., Hopkins, F. M., Yadav, V., Bue, B. D., Thompson, D. R., Conley, S., Colombi, N. K., Frankenberg, C., McCubbin, I. B., Eastwood, M. L., Falk, M., Herner, J. D., Croes, B. E., Green, R. O., and Miller, C. E.: California's methane super-emitters, Nature, 575, 180–184, https://doi.org/10.1038/s41586-019-1720-3, 2019.

887 Elvidge, C. D., Zhizhin, M., Baugh, K., Hsu, F.-C., and Ghosh, T.: Methods for Global Survey of Natural Gas Flaring
888 from Visible Infrared Imaging Radiometer Suite Data, Energies, 9, 14, https://doi.org/10.3390/en9010014, 2016.

889 ERG: City of Fort Worth Natural Gas Air Quality Study, Final Report, Eastern Research Group, Inc. (ERG), 2011.

890 Fox, T. A., Barchyn, T. E., Risk, D., Ravikumar, A. P., and Hugenholtz, C. H.: A review of close-range and screening
891 technologies for mitigating fugitive methane emissions in upstream oil and gas, Environ. Res. Lett., 14, 053002,
892 https://doi.org/10.1088/1748-9326/ab0cc3, 2019.

893 Goetz, J. D., Floerchinger, C., Fortner, E. C., Wormhoudt, J., Massoli, P., Knighton, W. B., Herndon, S. C., Kolb, C.
894 E., Knipping, E., Shaw, S. L., and DeCarlo, P. F.: Atmospheric Emission Characterization of Marcellus Shale Natural
895 Gas Development Sites, Environ. Sci. Technol., 49, 7012–7020, https://doi.org/10.1021/acs.est.5b00452, 2015.

896 de Gouw, J. A., Veefkind, J. P., Roosenbrand, E., Dix, B., Lin, J. C., Landgraf, J., and Levelt, P. F.: Daily Satellite
897 Observations of Methane from Oil and Gas Production Regions in the United States, Sci Rep, 10, 1379,
898 https://doi.org/10.1038/s41598-020-57678-4, 2020.

899 Jacob, D. J., Varon, D. J., Cusworth, D. H., Dennison, P. E., Frankenberg, C., Gautam, R., Guanter, L., Kelley, J.,
900 McKeever, J., Ott, L. E., Poulter, B., Qu, Z., Thorpe, A. K., Worden, J. R., and Duren, R. M.: Quantifying methane
901 emissions from the global scale down to point sources using satellite observations of atmospheric methane,
902 Atmospheric Chemistry and Physics, 22, 9617–9646, https://doi.org/10.5194/acp-22-9617-2022, 2022.

903 Johnson, M. R., Tyner, D. R., and Szekeres, A. J.: Blinded evaluation of airborne methane source detection using
904 Bridger Photonics LiDAR, Remote Sensing of Environment, 259, 112418, https://doi.org/10.1016/j.rse.2021.112418,
905 2021.

906 Kunkel, W. M., Carre-Burritt, A. E., Aivazian, G. S., Snow, N. C., Harris, J. T., Mueller, T. S., Roos, P. A., and
907 Thorpe, M. J.: Extension of Methane Emission Rate Distribution for Permian Basin Oil and Gas Production
908 Infrastructure by Aerial LiDAR, Environ. Sci. Technol., 57, 12234–12241, https://doi.org/10.1021/acs.est.3c00229,
909 2023.

910 Lan, X., Talbot, R., Laine, P., and Torres, A.: Characterizing Fugitive Methane Emissions in the Barnett Shale Area
911 Using a Mobile Laboratory, Environ. Sci. Technol., 49, 8139–8146, https://doi.org/10.1021/es5063055, 2015.

912 Lu, X., Jacob, D. J., Wang, H., Maasakkers, J. D., Zhang, Y., Scarpelli, T. R., Shen, L., Qu, Z., Sulprizio, M. P.,
913 Nesser, H., Bloom, A. A., Ma, S., Worden, J. R., Fan, S., Parker, R. J., Boesch, H., Gautam, R., Gordon, D., Moran,
914 M. D., Reuland, F., Villasana, C. A. O., and Andrews, A.: Methane emissions in the United States, Canada, and
915 Mexico: evaluation of national methane emission inventories and 2010–2017 sectoral trends by inverse analysis of in
916 situ (GLOBALVIEWplus CH$_4$ ObsPack) and satellite (GOSAT) atmospheric observations, Atmospheric Chemistry
917 and Physics, 22, 395–418, https://doi.org/10.5194/acp-22-395-2022, 2022.

918 Lu, X., Jacob, D. J., Zhang, Y., Shen, L., Sulprizio, M. P., Maasakkers, J. D., Varon, D. J., Qu, Z., Chen, Z., Hmiel,
919 B., Parker, R. J., Boesch, H., Wang, H., He, C., and Fan, S.: Observation-derived 2010-2019 trends in methane
920 emissions and intensities from US oil and gas fields tied to activity metrics, Proceedings of the National Academy of
921 Sciences, 120, e2217900120, https://doi.org/10.1073/pnas.2217900120, 2023.

922 Maasakkers, J. D., Jacob, D. J., Sulprizio, M. P., Scarpelli, T. R., Nesser, H., Sheng, J., Zhang, Y., Lu, X., Bloom, A.
923 A., Bowman, K. W., Worden, J. R., and Parker, R. J.: 2010–2015 North American methane emissions, sectoral
924 contributions, and trends: a high-resolution inversion of GOSAT observations of atmospheric methane, Atmospheric
925 Chemistry and Physics, 21, 4339–4356, https://doi.org/10.5194/acp-21-4339-2021, 2021.

926 Miller, S. M., Wofsy, S. C., Michalak, A. M., Kort, E. A., Andrews, A. E., Biraud, S. C., Dlugokencky, E. J.,
927 Eluszkiewicz, J., Fischer, M. L., Janssens-Maenhout, G., Miller, B. R., Miller, J. B., Montzka, S. A., Nehrkorn, T.,
928 and Sweeney, C.: Anthropogenic emissions of methane in the United States, Proceedings of the National Academy of
929 Sciences, 110, 20018–20022, https://doi.org/10.1073/pnas.1314392110, 2013.

930 Mitchell, A. L., Tkacik, D. S., Roscioli, J. R., Herndon, S. C., Yacovitch, T. I., Martinez, D. M., Vaughn, T. L.,
931 Williams, L. L., Sullivan, M. R., Floerchinger, C., Omara, M., Subramanian, R., Zimmerle, D., Marchese, A. J., and

932 Robinson, A. L.: Measurements of Methane Emissions from Natural Gas Gathering Facilities and Processing Plants:
933 Measurement Results, Environ. Sci. Technol., 49, 3219–3227, https://doi.org/10.1021/es5052809, 2015.

934 Nesser, H., Jacob, D. J., Maasakkers, J. D., Lorente, A., Chen, Z., Lu, X., Shen, L., Qu, Z., Sulprizio, M. P., Winter,
935 M., Ma, S., Bloom, A. A., Worden, J. R., Stavins, R. N., and Randles, C. A.: High-resolution U.S. methane emissions
936 inferred from an inversion of 2019 TROPOMI satellite data: contributions from individual states, urban areas, and
937 landfills, EGUsphere, 1–36, https://doi.org/10.5194/egusphere-2023-946, 2023.

938 Ocko, I. B., Sun, T., Shindell, D., Oppenheimer, M., Hristov, A. N., Pacala, S. W., Mauzerall, D. L., Xu, Y., and
939 Hamburg, S. P.: Acting rapidly to deploy readily available methane mitigation measures by sector can immediately
940 slow global warming, Environ. Res. Lett., 16, 054042, https://doi.org/10.1088/1748-9326/abf9c8, 2021.

941 Omara, M., Sullivan, M. R., Li, X., Subramanian, R., Robinson, A. L., and Presto, A. A.: Methane Emissions from
942 Conventional and Unconventional Natural Gas Production Sites in the Marcellus Shale Basin, Environ. Sci. Technol.,
943 50, 2099–2107, https://doi.org/10.1021/acs.est.5b05503, 2016.

944 Omara, M., Zimmerman, N., Sullivan, M. R., Li, X., Ellis, A., Cesa, R., Subramanian, R., Presto, A. A., and Robinson,
945 A. L.: Methane Emissions from Natural Gas Production Sites in the United States: Data Synthesis and National
946 Estimate, Environ. Sci. Technol., 52, 12915–12925, https://doi.org/10.1021/acs.est.8b03535, 2018.

947 Omara, M., Zavala-Araiza, D., Lyon, D. R., Hmiel, B., Roberts, K. A., and Hamburg, S. P.: Methane emissions from
948 US low production oil and natural gas well sites, Nat Commun, 13, 2085, https://doi.org/10.1038/s41467-022-29709-
949 3, 2022.

950 Omara, M., Himmelberger, A., MacKay, K., Williams, J. P., Benmergui, J., Sargent, M., Wofsy, S. C., and Gautam,
951 R.: Constructing a measurement-based spatially explicit inventory of US oil and gas methane emissions, Earth System
952 Science Data Discussions, 1–25, https://doi.org/10.5194/essd-2024-72, 2024.

953 Plant, G., Kort, E. A., Brandt, A. R., Chen, Y., Fordice, G., Gorchov Negron, A. M., Schwietzke, S., Smith, M., and
954 Zavala-Araiza, D.: Inefficient and unlit natural gas flares both emit large quantities of methane, Science, 377, 1566–
955 1571, https://doi.org/10.1126/science.abq0385, 2022.

956 Ravikumar, A. P., Wang, J., McGuire, M., Bell, C. S., Zimmerle, D., and Brandt, A. R.: "Good versus Good Enough?"
957 Empirical Tests of Methane Leak Detection Sensitivity of a Commercial Infrared Camera, Environ. Sci. Technol., 52,
958 2368–2374, https://doi.org/10.1021/acs.est.7b04945, 2018.

959 Rella, C. W., Hoffnagle, J., He, Y., and Tajima, S.: Local- and regional-scale measurements of CH_4, $\delta^{13}CH_4$, and C_2H_6
960 in the Uintah Basin using a mobile stable isotope analyzer, Atmospheric Measurement Techniques, 8, 4539–4559,
961 https://doi.org/10.5194/amt-8-4539-2015, 2015.

962 Riddick, S. N., Mauzerall, D. L., Celia, M. A., Kang, M., Bressler, K., Chu, C., and Gum, C. D.: Measuring methane
963 emissions from abandoned and active oil and gas wells in West Virginia, Science of The Total Environment, 651,
964 1849–1856, https://doi.org/10.1016/j.scitotenv.2018.10.082, 2019.

965 Riddick, S. N., Ancona, R., Mbua, M., Bell, C. S., Duggan, A., Vaughn, T. L., Bennett, K., and Zimmerle, D. J.: A
966 quantitative comparison of methods used to measure smaller methane emissions typically observed from
967 superannuated oil and gas infrastructure, Atmospheric Measurement Techniques, 15, 6285–6296,
968 https://doi.org/10.5194/amt-15-6285-2022, 2022.

969 Riddick, S. N., Mbua, M., Santos, A., Emerson, E. W., Cheptonui, F., Houlihan, C., Hodshire, A. L., Anand, A.,
970 Hartzell, W., and Zimmerle, D. J.: Methane emissions from abandoned oil and gas wells in Colorado, Science of The
971 Total Environment, 922, 170990, https://doi.org/10.1016/j.scitotenv.2024.170990, 2024.

972 Robertson, A. M., Edie, R., Snare, D., Soltis, J., Field, R. A., Burkhart, M. D., Bell, C. S., Zimmerle, D., and Murphy,
973 S. M.: Variation in Methane Emission Rates from Well Pads in Four Oil and Gas Basins with Contrasting Production
974 Volumes and Compositions, Environ. Sci. Technol., 51, 8832–8840, https://doi.org/10.1021/acs.est.7b00571, 2017.

975 Robertson, A. M., Edie, R., Field, R. A., Lyon, D., McVay, R., Omara, M., Zavala-Araiza, D., and Murphy, S. M.:
976 New Mexico Permian Basin Measured Well Pad Methane Emissions Are a Factor of 5–9 Times Higher Than U.S.
977 EPA Estimates, Environ. Sci. Technol., 54, 13926–13934, https://doi.org/10.1021/acs.est.0c02927, 2020.

978 Rutherford, J. S., Sherwin, E. D., Ravikumar, A. P., Heath, G. A., Englander, J., Cooley, D., Lyon, D., Omara, M.,
979 Langfitt, Q., and Brandt, A. R.: Closing the methane gap in US oil and natural gas production emissions inventories,
980 Nat Commun, 12, 4715, https://doi.org/10.1038/s41467-021-25017-4, 2021.

981 Shen, L., Gautam, R., Omara, M., Zavala-Araiza, D., Maasakkers, J. D., Scarpelli, T. R., Lorente, A., Lyon, D., Sheng,
982 J., Varon, D. J., Nesser, H., Qu, Z., Lu, X., Sulprizio, M. P., Hamburg, S. P., and Jacob, D. J.: Satellite quantification
983 of oil and natural gas methane emissions in the US and Canada including contributions from individual basins,
984 Atmospheric Chemistry and Physics, 22, 11203–11215, https://doi.org/10.5194/acp-22-11203-2022, 2022.

985 Sherwin, E., Zhang, Z., Chen, Y., Wetherley, E. B., Yakovlev, P., Berman, E. S. F., Jones, B. B., Thorpe, A. K.,
986 Ayasse, A. K., Duren, R., Brandt, A. R., and Cusworth, D. H.: Quantifying oil and natural gas system emissions using
987 one million aerial site measurements, https://doi.org/10.21203/rs.3.rs-2406848/v1, 2023a.

988 Sherwin, E. D., Rutherford, J. S., Chen, Y., Aminfard, S., Kort, E. A., Jackson, R. B., and Brandt, A. R.: Single-blind
989 validation of space-based point-source detection and quantification of onshore methane emissions, Sci Rep, 13, 3836,
990 https://doi.org/10.1038/s41598-023-30761-2, 2023b.

991 Sherwin, E. D., Rutherford, J. S., Zhang, Z., Chen, Y., Wetherley, E. B., Yakovlev, P. V., Berman, E. S. F., Jones, B.
992 B., Cusworth, D. H., Thorpe, A. K., Ayasse, A. K., Duren, R. M., and Brandt, A. R.: US oil and gas system emissions
993 from nearly one million aerial site measurements, Nature, 627, 328–334, https://doi.org/10.1038/s41586-024-07117-
994 5, 2024.

995 Stavropoulou, F., Vinković, K., Kers, B., de Vries, M., van Heuven, S., Korbeń, P., Schmidt, M., Wietzel, J., Jagoda,
996 P., Necki, J. M., Bartyzel, J., Maazallahi, H., Menoud, M., van der Veen, C., Walter, S., Tuzson, B., Ravelid, J.,
997 Morales, R. P., Emmenegger, L., Brunner, D., Steiner, M., Hensen, A., Velzeboer, I., van den Bulk, P., Denier van
998 der Gon, H., Delre, A., Edjabou, M. E., Scheutz, C., Corbu, M., Iancu, S., Moaca, D., Scarlat, A., Tudor, A., Vizireanu,
999 I., Calcan, A., Ardelean, M., Ghemulet, S., Pana, A., Constantinescu, A., Cusa, L., Nica, A., Baciu, C., Pop, C.,
1000 Radovici, A., Mereuta, A., Stefanie, H., Dandocsi, A., Hermans, B., Schwietzke, S., Zavala-Araiza, D., Chen, H., and
1001 Röckmann, T.: High potential for CH_4 emission mitigation from oil infrastructure in one of EU's major production
1002 regions, Atmospheric Chemistry and Physics, 23, 10399–10412, https://doi.org/10.5194/acp-23-10399-2023, 2023.

1003 Thorpe, M. J., Krietinger, A., Altamura, D., Dudiak, C. D., Conrad, B. M., Tyner, D. R., Johnson, M. R., Brasseur, J.
1004 K., Roos, P., Kunkel, W., Carre-Burritt, A., Abate, J., Price, T., Yaralian, D., Kennedy, B., Newton, E., Rodriguez,
1005 E., Elfar, O. I., and Zimmerle, D. J.: Deployment-invariant probability of detection characterization for aerial LiDAR
1006 methane detection, 2024.

1007 Tyner, D. R. and Johnson, M. R.: Where the Methane Is—Insights from Novel Airborne LiDAR Measurements
1008 Combined with Ground Survey Data, Environ. Sci. Technol., 55, 9773–9783, https://doi.org/10.1021/acs.est.1c01572,
1009 2021.

1010 Inventory of U.S. Greenhouse Gas Emissions and Sinks: https://www.epa.gov/ghgemissions/inventory-us-
1011 greenhouse-gas-emissions-and-sinks, last access: 6 March 2024.

1012 EPA's Final Rule for Oil and Natural Gas Operations Will Sharply Reduce Methane and Other Harmful Pollution.:
1013 https://www.epa.gov/controlling-air-pollution-oil-and-natural-gas-operations/epas-final-rule-oil-and-natural-gas, last
1014 access: 5 March 2024.

1015 Weller, Z. D., Hamburg, S. P., and von Fischer, J. C.: A National Estimate of Methane Leakage from Pipeline Mains
1016 in Natural Gas Local Distribution Systems, Environ. Sci. Technol., 54, 8958–8967,
1017 https://doi.org/10.1021/acs.est.0c00437, 2020.

1018 Williams, J. P., Regehr, A., and Kang, M.: Methane Emissions from Abandoned Oil and Gas Wells in Canada and the
1019 United States, Environ. Sci. Technol., 55, 563–570, https://doi.org/10.1021/acs.est.0c04265, 2021.

1020 Williams, J. P., El Hachem, K., and Kang, M.: Controlled-release testing of the static chamber methodology for direct
1021 measurements of methane emissions, Atmospheric Measurement Techniques, 16, 3421–3435,
1022 https://doi.org/10.5194/amt-16-3421-2023, 2023.

1023 Worden, J. R., Cusworth, D. H., Qu, Z., Yin, Y., Zhang, Y., Bloom, A. A., Ma, S., Byrne, B. K., Scarpelli, T.,
1024 Maasakkers, J. D., Crisp, D., Duren, R., and Jacob, D. J.: The 2019 methane budget and uncertainties at 1° resolution
1025 and each country through Bayesian integration Of GOSAT total column methane data and a priori inventory estimates,
1026 Atmospheric Chemistry and Physics, 22, 6811–6841, https://doi.org/10.5194/acp-22-6811-2022, 2022.

1027 Xia, H., Strayer, A., and Ravikumar, A. P.: The Role of Emission Size Distribution on the Efficacy of New
1028 Technologies to Reduce Methane Emissions from the Oil and Gas Sector, Environ. Sci. Technol., 58, 1088–1096,
1029 https://doi.org/10.1021/acs.est.3c05245, 2024.

1030 Yacovitch, T. I., Herndon, S. C., Pétron, G., Kofler, J., Lyon, D., Zahniser, M. S., and Kolb, C. E.: Mobile Laboratory
1031 Observations of Methane Emissions in the Barnett Shale Region, Environ. Sci. Technol., 49, 7889–7895,
1032 https://doi.org/10.1021/es506352j, 2015.

1033 Zhang, Y., Gautam, R., Pandey, S., Omara, M., Maasakkers, J. D., Sadavarte, P., Lyon, D., Nesser, H., Sulprizio, M.
1034 P., Varon, D. J., Zhang, R., Houweling, S., Zavala-Araiza, D., Alvarez, R. A., Lorente, A., Hamburg, S. P., Aben, I.,
1035 and Jacob, D. J.: Quantifying methane emissions from the largest oil-producing basin in the United States from space,
1036 Science Advances, 6, eaaz5120, https://doi.org/10.1126/sciadv.aaz5120, 2020.

1037 Zhou, X., Yoon, S., Mara, S., Falk, M., Kuwayama, T., Tran, T., Cheadle, L., Nyarady, J., Croes, B., Scheehle, E.,
1038 Herner, J. D., and Vijayan, A.: Mobile sampling of methane emissions from natural gas well pads in California,
1039 Atmospheric Environment, 244, 117930, https://doi.org/10.1016/j.atmosenv.2020.117930, 2021.

1040 Zimmerle, D., Vaughn, T., Luck, B., Lauderdale, T., Keen, K., Harrison, M., Marchese, A., Williams, L., and Allen,
1041 D.: Methane Emissions from Gathering Compressor Stations in the U.S., Environ. Sci. Technol., 54, 7552–7561,
1042 https://doi.org/10.1021/acs.est.0c00516, 2020.

1043

1044

1045

1046

1047

1048

1049

1050